J. Fluid Mech. (2008), *vol.* 597, *pp.* 199–231.
doi:10.1017/S0022112007009676 Printed in the United Kingdom

Feasibility, efficiency and transportability of short-horizon optimal mixing protocols

LUCA CORTELEZZI[1]†, ALESSANDRA ADROVER[2] AND MASSIMILIANO GIONA[2]

[1]Department of Mechanical Engineering, McGill University, Montreal, Canada

[2]Dipartimento di Ingegneria Chimica, Università di Roma 'La Sapienza', Rome, Italy

(Received 13 December 2006 and in revised form 24 October 2007)

We consider, as a case study, the optimization of mixing protocols for a two-dimensional, piecewise steady, nonlinear flow, the sine flow, for both the advective–diffusive and purely advective cases. We use the mix-norm as the cost function to be minimized by the optimization procedure. We show that the cost function possesses a complex structure of local minima of nearly the same values and, consequently, that the problem possesses a large number of sub-optimal protocols with nearly the same mixing efficiency as the optimal protocol. We present a computationally efficient optimization procedure able to find a sub-optimal protocol through a sequence of short-time-horizon optimizations. We show that short-time-horizon optimal mixing protocols, although sub-optimal, are both feasible and efficient at mixing flows with and without diffusion. We also show that these optimized protocols can be derived, at lower computational cost, for purely advective flows and successfully transported to advective–diffusive flows with small molecular diffusivity. We characterize our results by discussing the asymptotic properties of the optimized protocols both in the pure advection and in the advection–diffusion cases. In particular, we quantify the mixing efficiency of the optimized protocols using the Lyapunov exponents and Poincaré sections for the pure advection case, and the eigenvalue–eigenfunction spectrum for the advection–diffusion case. Our results indicate that the optimization over very short-time horizons could in principle be used as an on-line procedure for enhancing mixing in laboratory experiments, and in future engineering applications.

1. Introduction

The optimization and control of fluid mixing is highly relevant to modern and future industrial applications, because the demands for improving the efficiency of mixing processes and controlling the homogeneity of mixtures are becoming increasingly severe. A better understanding of mixing is crucial for improving old and designing novel mixing devices that are able to reduce residence mixing times, improve mixing homogeneity and allow the processing of new materials highly sensitive to concentration and temperature gradients.

There are several potential techniques for enhancing mixing. They range from off-line optimization and passive control to on-line optimization and feedback control. On the one hand, off-line optimization and passive control are the most

† Author to whom correspondence should be addressed: crtlz@cim.mcgill.ca; also affiliated with the Dipartimento di Fisica, Università di Udine, 33100 Udine, Italia.

robust techniques, but they are strongly dependent on process, geometry and application. On the other hand, on-line optimization and feedback control are hard to design and require a deep understanding of the mixing process, but they are versatile and adaptable to different processes, geometries and applications.

Over the past two decades, mixing protocols have been devised to induce chaotic advection, also referred to as *Lagrangian chaos* or *laminar chaos*, in laminar flows when the mixing properties of turbulence cannot be leveraged. More recently, the swiftly developing area of microfluidic technology (Tay 2002; Tabeling 2005) has introduced the new challenge of mixing laminar flows in micro-channels where the characteristic length of the channel is often comparable to the characteristic diffusion length of the fluids. Several studies have recently been published on this subject, both from the theoretical–numerical and the experimental standpoints (see e.g. Stremler, Haselton & Aref 2004; Tabeling *et al.* 2004; Ottino & Wiggins 2004*a*, 2004*b*, and references cited therein).

Most of the research activity in the mixing community has focused on the analysis of the mixing efficiency of stirring protocols applied to purely advective flows. The types of flows considered range from idealized flow models, used as computationally convenient playgrounds for achieving a basic understanding of the advective mixing mechanisms (Rom-Kedar, Leonard & Wiggins 1990; Beigie, Leonard & Wiggins 1994; Hobbs, Alvarez & Muzzio 1997), to industrially relevant flows, such as those arising in stirred vessels (Lamberto *et al.* 1996; Harvey III, Wood & Leng 1997; Alvarez *et al.* 2002*b*; Rice *et al.* 2006) and motionless mixers (Zalc, Szalai & Muzzio 2003; Hobbs & Muzzio 1998; Metcalfe *et al.* 2005; Xia *et al.* 2006). These studies were complemented by carefully designed numerical and laboratory experiments of two- and three-dimensional Stokes flows, such as the flow between two eccentric rotating cylinders, the flow in a rectangular cavity driven by sliding walls (Ottino 1989), and the flow in a cylindrical vessel stirred by tilted (Fountain, Khakhar & Ottino 1997) or eccentric disks (Alvarez, Arratia & Muzzio 2002*a*). The main result of these studies can be summarized by saying that optimal stirring protocols are those which maximize the amount of chaos in the flow domain, i.e. maximize the measure of the set of trajectories possessing positive maximal Lyapunov exponent. Consequently, the presence of regions of regular motion, known as *islands* in two-dimensional flows and *invariant tori* in three-dimensional flows, should be avoided, as they form a barrier to efficient mixing. Unfortunately, besides a handful of abstract systems which are weakly related to fluid mixing (see e.g. the class of models analysed in Wojtkowski 1981), there is no simple way of establishing *a priori* the shape and the size of the regions of regular motion which are associated with a prescribed stirring protocol.

Along this line of research, a comparatively smaller number of studies focus on optimizing or controlling mixing (Franjione & Ottino 1992; Sharma & Gupte 1997; D'Alessandro, Dahleh & Mezić 1999; Boyland, Aref & Stremler 2000; Vikhansky 2002*a*, *b*; Balasuriya 2005; Thiffeault & Finn 2006). The results obtained, however, differ, and are hard to compare because they strongly depend on the definition of mixing efficiency and mixing quality chosen by the different authors. For instance, D'Alessandro *et al.* (1999) quantify mixing quality in terms of measure-theoretical entropy. The authors used this quantity to identify the most effective protocol out of a generic sequence of orthogonal shear flows on a two-dimensional torus. While theoretically satisfactory, this definition is hardly suitable for engineering applications. In other theoretical–numerical studies, which considered more realistic flows, the mixing efficiency of a given protocol was assessed in terms of the stretch factor of

the passive interfaces evolving under the action of the protocol (see e.g. Vikhansky 2002*a*, *b*). Balasuriya (2005) considered the mixing enhancement induced by periodic perturbations of two- and three-dimensional axis-symmetric integrable flows as a function of the frequency of the perturbation. In this case, mixing enhancement is quantified through the mass flux across the separatrix associated with the unperturbed system: such flux is clearly zero in the unperturbed cases. A first attempt at feedback control mixing has been recently presented by Noack *et al.* (2004). In this work, the authors developed a variational approach for controlling the dynamics of a vortex, providing a low-frequency modulation of the vortex motion and quantifying mixing performances by the use of Poincaré maps. Note that all of the aforementioned optimization and control studies use kinematics-based diagnostics to quantify mixing efficiency. More recently, Mathew *et al.* (2007) considered the problem of optimally controlling mixing in a Stokes flow by modulating a finite set of spatially distributed force fields. The authors derived the first-order necessary conditions for optimality and obtained a sub-optimal controller using a conjugate gradient algorithm.

The scope of this study is to investigate the feasibility, efficiency and transportability of short-time-horizon optimal mixing protocols. We are particularly interested in assessing the feasibility and efficiency of such protocols when the optimization horizon is short with respect to the characteristic advection time of the system. A positive assessment could have important implications for engineering applications since on-line optimization could be effectively integrated in novel mixing devices. Furthermore, our study analyses whether short-time-horizon optimal protocols can be designed and tested on purely advective flows, and subsequently transported to advective–diffusive flows, without a substantial deterioration of their mixing efficiency. To the best of our knowledge, there are no studies published investigating these types of protocols.

In order to characterize the mixing efficiency of short-time-horizon optimal mixing protocols when applied to purely advective or advective–diffusive systems, it is necessary to introduce diagnostics able to quantify the quality of mixing on either system. The typical indicators of the quality of mixing, i.e. variance decay exponent and kinematics-based diagnostics, are unhelpful in our analysis because they cannot be used interchangeably for purely advective and advective–diffusive systems. On the one hand, the scalar variance is conserved in diffusionless systems, independently of the efficiency of the advective mixing. On the other hand, in advecting–diffusing flows, the interfaces between fluids cannot be clearly identified due to the smearing action of diffusion and, consequently, all the diagnostics based on the dynamics of local and global deformation of passive interfaces are bound to be imprecise.

Recently, Mathew *et al.* (2005) proposed a global indicator of the degree of mixing, the mix-norm, which can be used to characterize mixing in flows with or without molecular diffusion. The mix-norm is essentially an average multiscale measure of the scalar variance over different coarse grainings of the mixing domain, obtained by first averaging the concentration field over measure elements of a characteristic length scale centred at a generic point of the mixing domain, and then taking the average of the square of this quantity with respect to the space coordinates.

In this study, we use the mix-norm, we believe for the first time, to quantify the mixing efficiency of protocols when applied to purely advective or advective–diffusive systems. We search for optimal protocols that minimize the mix-norm out of a pool of admissible protocols for a test flow, the sine flow (Liu, Muzzio & Peskin 1994*a*). The

sine flow has been widely used as a computationally convenient model for analysing chaotic advection induced by aperiodic protocols (Liu *et al.* 1994*a*), the interaction between the advective and diffusive mixing mechanisms (Giona *et al.* 2004*b*; Thiffeault, Doering & Gibbon 2004) and the evolution of advecting–diffusing–reacting systems (see e.g. Giona, Cerbelli & Adrover 2002).

The third issue we investigate in this study is the transportability of a protocol, optimized in the absence of diffusion, from purely advective to advective–diffusive systems. It is not trivial to answer the question as to whether optimal protocols designed for purely advective flows also perform best in the presence of diffusion, however small. This question is important because diffusionless systems are physically unattainable. Some researchers tend to answer this question by saying that if a flow field provides efficient advective mixing and molecular diffusion is small, then the action of molecular diffusion can be superimposed an the advective flow, and therefore the assessment of mixing optimality obtained from the kinematic analysis can be relied on. In general, however, this is not true. Direct numerical simulations of advecting–diffusing scalar fields in two- and three-dimensional flows show that the interaction between chaotic advection and molecular diffusion can give rise to a rich variety of phenomenological behaviours such as the localization of partially mixed structures within regions of regular motion in the mixing space (Giona, Cerbelli & Vitacolonna 2004*a*). For small diffusivities, these phenomenological behaviours are characterized by exponential scaling laws, where the value of the exponent is an indicator of qualitatively different transport mechanisms (see e.g. Toussaint, Carriere & Raynal 1995; Toussaint *et al.* 2000; Giona *et al.* 2004*b*; Cerbelli *et al.* 2004). In practice, in partially mixing flows, the complex interaction between chaotic advection and diffusion is essentially related to the possible presence of regions of regular motion, i.e. islands or invariant tori, intermingled with regions of chaotic motion. In these cases, the overall mixing efficiency depends on how the chaotic region mediates the transport between regions of regular motion (Giona *et al.* 2004*b*). Note that the regions of regular motion are not detected by global indicators of chaos such as Lyapunov exponents or topological entropy. In fact, these indicators are ultimately based on local stretch factors and are therefore dominated by the exponential dynamics of deformation occurring in the chaotic region.

The remainder of this article is organized as follows: In § 2, we illustrate the sine flow and the admissible protocols. We define a protocol as optimal if it minimizes the mix-norm of the scalar field at a given final time. We determine an optimal protocol by performing an exhaustive search between all possible protocols. We perform the optimizations over horizons ranging from very small to large time intervals, in order to characterize the mixing efficiency of very short-horizon mixing protocols. In § 3, the results of the short-time-horizon optimization are discussed. Optimal protocols derived for diffusionless flows are compared with optimal protocols derived for advection–diffusion flows. Furthermore, the transportability of optimal protocols derived for diffusionless flows to advection–diffusion flows is discussed. In § 4, we analyse the kinematic and functional properties of the short-horizon optimal protocols and their fine temporal structure. In particular, we observe that the results of the kinematics-based optimization can be used with confidence even in the presence of a small molecular diffusivity if the repeated application of the protocol optimized over a short time horizon, henceforth referred to as the *periodic continuation* of the protocol, induces a globally chaotic flow. Concluding remarks and possible developments of the approach presented are discussed in § 5.

2. Statement of the problem and optimization strategy

2.1. *Flow system and admissible protocols*

We use the sine flow (Liu *et al.* 1994*a*) as a test flow system to derive and compare optimal protocols acting on purely advecting and advecting–diffusing scalar fields. The sine flow is defined as a two-dimensional, incompressible fluid system stirred by the composition of two blinking, piecewise steady, nonlinear velocity fields,

$$\boldsymbol{v}_0(x, y) = (\sin(2\pi y), 0), \quad \boldsymbol{v}_1(x, y) = (0, \sin(2\pi x)), \tag{2.1}$$

acting on all points of a unit square domain $I^2 = [0, 1] \times [0, 1]$ equipped with periodic boundary conditions which identify the opposite edges of the square. Note that the flow domain is topologically equivalent to a two-dimensional torus, $\mathbb{T}^2$.

It is physically meaningful to blink the velocity fields only if we assume flow conditions for which the inertial effects are negligible with respect to the viscous effects. Liu *et al.* (1994*b*) have characterized the impact of the inertial effects on the mixing properties of laminar chaotic flows. They considered a two-dimensional cavity flow in which the chaotic flow is obtained by alternating the motion of the upper and lower walls of the cavity. Liu *et al.* (1994*b*) observed that for Reynolds numbers less than one, the kinematic of mixing can be reproduced numerically by blinking the steady-state solutions to the Stokes equations corresponding to the motion of the upper or lower walls of the cavity. They showed that the kinematics reproduced by blinking the two solutions is a sufficiently accurate approximation of the kinematics obtained by solving the corresponding continuous-time problem governed by the Navier–Stokes equations.

Under the above assumption, we stir the sine flow system with a set of admissible protocols defined as follows. Let T be the overall time interval over which the optimization is performed, and let $\tau = T/N$ be a switching time, where N is a positive integer. An *admissible protocol* is a string $\{\alpha_1, \alpha_2, \ldots, \alpha_N\}$ which prescribes the stirring velocity field as a sequence of N instantaneously switching flows $\{\boldsymbol{v}_{\alpha_1}, \boldsymbol{v}_{\alpha_2}, \ldots, \boldsymbol{v}_{\alpha_N}\}$, each acting over a time τ, where α_i can be either '0' or '1' for $i = 1, 2, \ldots, N$. Note that all protocols possess the same kinetic energy.

Although defined on a boundary-less manifold, the two-dimensional torus $\mathbb{T}^2$, the sine flow represents a bounded closed flow system, since the flow domain can be embedded in a finite-size ball. No leakage of fluid can occur because there are no boundaries. Consequently, the evolution of a scalar field shares the same properties as the evolution of an incompressible fluid enclosed between bounded impermeable walls (Giona *et al.* 2004*b*).

2.2. *Solution of the advection–diffusion problem*

Advection–diffusion of a scalar, or concentration, field $\phi(x, y, t)$ is governed by the dimensionless equation

$$\frac{\partial \phi}{\partial t} = -\boldsymbol{v} \cdot \nabla \phi + \frac{1}{Pe} \Delta \phi, \tag{2.2}$$

where $\boldsymbol{v}(x, y, t) = \boldsymbol{v}_{\alpha_i}(x, y)/U$ for $(i-1)\tau \leqslant t < i\tau$ $(i = 1, 2, \ldots, N)$ is a solenoidal velocity field, i.e. $\nabla \cdot \boldsymbol{v} = 0$, and Δ represents the Laplacian operator. The Péclet number is defined as $Pe = UL/\mathscr{D}$, where U, L, $\mathscr{D}$ are the characteristic velocity, characteristic length, and molecular diffusivity, respectively. As a characteristic velocity U and length L, we choose the maximum absolute value of the stirring velocity field and the side of the square domain, respectively. We also define the characteristic advection time as $T_K = L/U$ and the characteristic diffusion time as $T_D = L^2/\mathscr{D}$. Note that the

Péclet number can also be expressed as $Pe = T_D/T_K$. Hence, the role of fluid motion increases with increasing Pe.

The advection–diffusion equation (2.2) can be conveniently solved using a spectral algorithm. Let us expand the scalar field in terms of the Fourier orthonormal basis, i.e.

$$\phi(x, y, t) = \sum_{\boldsymbol{k}\in\mathbb{Z}^2} \Phi_{\boldsymbol{k}}(t)\, \mathrm{e}^{2\mathrm{i}\pi\, \boldsymbol{k}\cdot\boldsymbol{x}}, \tag{2.3}$$

where $\boldsymbol{k} = (m, n) \in \mathbb{Z}^2$ is the wavenumber vector ($\mathbb{Z}^2$ is the set of points of the plane possessing positive, null, or negative integer coordinates), $\boldsymbol{x} = (x, y)$ is the position vector, and $\mathrm{i} = \sqrt{-1}$, respectively. Since the scalar field is real-valued, the coefficients of the Fourier expansion, $\Phi_{\boldsymbol{k}}(t)$, always appear in complex-conjugate pairs. Using a Galerkin projection scheme, we obtain the following infinite-dimensional system of ordinary differential equations for the Fourier coefficients $\Phi_{\boldsymbol{k}}(t) = \Phi_{m,n}(t)$,

$$\frac{\mathrm{d}\Phi_{m,n}(t)}{\mathrm{d}t} = -\frac{4\pi^2(m^2+n^2)}{Pe}\Phi_{m,n}(t) - \pi m(\Phi_{m,n-1}(t) - \Phi_{m,n+1}(t)), \quad \forall (m, n) \in \mathbb{Z}^2, \tag{2.4}$$

for the time intervals when the stirring flow $\boldsymbol{v}_0 = (\sin(2\pi y), 0)$ is active, and the infinite-dimensional system of ordinary differential equations

$$\frac{\mathrm{d}\Phi_{m,n}(t)}{\mathrm{d}t} = -\frac{4\pi^2(m^2+n^2)}{Pe}\Phi_{m,n}(t) - \pi n(\Phi_{m-1,n}(t) - \Phi_{m+1,n}(t)), \quad \forall (m, n) \in \mathbb{Z}^2, \tag{2.5}$$

for the time intervals when the stirring flow $\boldsymbol{v}_1 = (0, \sin(2\pi x))$ is active.

The presence of the dissipative Laplacian term in the above equations (first term on the right-hand side) ensures that a truncated Fourier representation of the scalar field ϕ provides an approximated solution to the infinite-dimensional system of ordinary differential equations (2.4)–(2.5). The validity of the truncated representation is supported by the fact that the evolution operator associated with the advection–diffusion equation is compact (Liu & Haller 2004; Cerbelli *et al.* 2004). Hence, we consider a finite set of wavenumbers $\boldsymbol{k} \in [-N_m, N_m] \times [-N_m, N_m]$. In order to maintain a good approximation to the solution, the number of modes N_m, which should be used in each spatial direction, should increase as Pe increases. We use $N_m = 50$ for $Pe = 10^3$ and $Pe = 5 \times 10^3$, $N_m = 70$ for $Pe = 10^4$, and $N_m = 120$ for $Pe = 5 \times 10^4$. The initial condition specifying the Cauchy problem for equations (2.4)–(2.5) is obtained by computing the Fourier coefficients of the initial scalar field $\phi(x, y, 0)$. The time integration is performed with a Runge–Kutta fourth-order algorithm.

2.3. *Solution of the pure advection problem*

Pure advection of a scalar field $\phi(x, y, t)$ is governed by the dimensionless equation

$$\frac{\partial\phi}{\partial t} = -\boldsymbol{v}\cdot\nabla\phi. \tag{2.6}$$

This equation is obtained from (2.2) by removing the diffusive term $\Delta\phi/Pe$. We identify this case with $Pe = \infty$. The Lagrangian form of the above equation is

$$\frac{\mathrm{D}\phi}{\mathrm{D}t} = 0, \tag{2.7}$$

where $\mathrm{D}/\mathrm{D}t$ is the material derivative. From this equation, it follows that the concentration is conserved in time, i.e. the concentration initially associated with a fluid particle remains constant as the particle is advected through the fluid by the velocity field $\boldsymbol{v}$. Consequently, the time evolution of the concentration field in the absence of diffusion can be easily obtained from the time evolution of the fluid particles.

The trajectory $(X(t), Y(t))$ traced by a fluid particle initially located at (X_0, Y_0) under the action of the velocity field $\boldsymbol{v}_0$ can be obtained integrating the following set of ordinary differential equations

$$\frac{\mathrm{d}X}{\mathrm{d}t} = \sin(2\pi Y), \quad \frac{\mathrm{d}Y}{\mathrm{d}t} = 0. \tag{2.8}$$

Hence, the position (X_1, Y_1) of the particle after one switching time τ is

$$\begin{cases} X_1 = X(\tau) = X_0 + \tau \sin(2\pi Y_0) & \mod 1, \\ Y_1 = Y(\tau) = Y_0 & \mod 1. \end{cases} \tag{2.9}$$

Note that we force the solution to evolve on a two-dimensional torus by taking the solution module one. Similarly, the trajectory $(X(t), Y(t))$ traced by a fluid particle initially located at (X_1, Y_1) under the action of the velocity field $\boldsymbol{v}_1$ can be obtained by integrating the following set of ordinary differential equations:

$$\frac{\mathrm{d}X}{\mathrm{d}t} = 0, \quad \frac{\mathrm{d}Y}{\mathrm{d}t} = \sin(2\pi X). \tag{2.10}$$

The position (X_2, Y_2) of the particle at time $t = 2\tau$ is

$$\begin{cases} X_2 = X(2\tau) = X_1 & \mod 1, \\ Y_2 = Y(2\tau) = Y_1 + \tau \sin(2\pi X_1) & \mod 1, \end{cases} \tag{2.11}$$

and so on. Therefore the stroboscopic kinematics of the fluid particle induced by a given protocol $\{\alpha_1, \alpha_2, \ldots, \alpha_N\}$, which prescribes the stirring velocity field as a sequence of N instantaneously switching flows $\{\boldsymbol{v}_{\alpha_1}, \boldsymbol{v}_{\alpha_2}, \ldots, \boldsymbol{v}_{\alpha_N}\}$, each acting over a time τ, is given by the map

$$\begin{pmatrix} X_k \\ Y_k \end{pmatrix} = \begin{cases} \begin{pmatrix} X_{k-1} + \tau \sin(2\pi Y_{k-1}) \\ Y_{k-1} \end{pmatrix} \mod 1 & \text{if} \quad \alpha_k = 0, \\ \begin{pmatrix} X_{k-1} \\ Y_{k-1} + \tau \sin(2\pi X_{k-1}) \end{pmatrix} \mod 1 & \text{if} \quad \alpha_k = 1, \end{cases} \tag{2.12}$$

where $k = 1, 2, \ldots, N$.

The solution to (2.6) can be easily obtained by inverting the stroboscopic map (2.12) describing the kinematics of the fluid particles. Since there is no diffusion, the initial concentration associated with a fluid particle is conserved with time. Hence, the solution to (2.6) at the point (x, y) and time $t = k\tau$ is

$$\phi(x, y, k\tau) = \phi(X_0, Y_0, 0), \quad k = 1, 2, \ldots, N, \tag{2.13}$$

where the position (X_0, Y_0) is obtained by setting $(X_k, Y_k) = (x, y)$ and using the map

$$\begin{pmatrix} X_{k-1} \\ Y_{k-1} \end{pmatrix} = \begin{cases} \begin{pmatrix} X_k - \tau \sin(2\pi Y_k) \\ Y_k \end{pmatrix} \mod 1 & \text{if} \quad \alpha_k = 0, \\ \begin{pmatrix} X_k \\ Y_k - \tau \sin(2\pi X_k) \end{pmatrix} \mod 1 & \text{if} \quad \alpha_k = 1, \end{cases} \tag{2.14}$$

to track the particle backward in time to its initial position.

2.4. *Definition and computation of the mix-norm*

As discussed in the introduction, the mix-norm (Mathew *et al.* 2005) provides a useful tool for quantifying the degree of mixing of an evolving scalar field over the entire range of Péclet numbers, including the value $Pe = \infty$, which represents a purely advective process.

The mix-norm can be defined as follows: Given a concentration field $\phi(\boldsymbol{x}, t)$ on a two-dimensional torus $\mathbb{T}^2$, the average of the concentration field $\phi(\boldsymbol{x}, t)$ over a ball $B_s(\boldsymbol{y}) = \{\boldsymbol{x} \mid \|\boldsymbol{x} - \boldsymbol{y}\| \leqslant s\}$ of radius s centred at $\boldsymbol{y}$, is

$$\mathrm{d}(\boldsymbol{y}, s, t) = \frac{1}{s} \int_{B_s(\boldsymbol{y})} \phi(\boldsymbol{x}, t)\, \mathrm{d}\boldsymbol{x}. \tag{2.15}$$

Then the mix-norm μ_ϕ is the square root of the average of $\mathrm{d}^2(\boldsymbol{y}, s, t)$ over all possible ball sizes and over the flow domain $\mathbb{T}^2$, i.e.

$$\mu_\phi(t) = \sqrt{\int_{\mathbb{T}^2} \left(\int_0^1 \mathrm{d}^2(\boldsymbol{y}, s, t)\, \mathrm{d}s \right) \mathrm{d}\boldsymbol{y}}. \tag{2.16}$$

It can be shown (Mathew *et al.* 2005) that this definition of the mix-norm is equivalent to the Sobolev norm of order $-1/2$ of $\phi(\boldsymbol{x}, t)$.

The mix-norm quantifies the mixedness of a concentration field both in purely advective and in advective–diffusive systems. In a diffusionless system, i.e. a system where the evolution of the concentration field is governed by (2.6), it can be shown (Mathew *et al.* 2005) that a stirring protocol mixes the initial concentration field in the measure-theoretical sense (Arnold & Avez 1989) if the mix-norm of $\phi(\boldsymbol{x}, t)$, evolved by (2.6), converges to zero for $t \to \infty$ for any initial square summable distribution. Conversely, in a system with diffusion, i.e. a system where the evolution of the concentration field is governed by (2.2), the mix-norm provides a quantification of mixedness alternative, but qualitatively equivalent, to the variance of the concentration field $\|\phi - \overline{\phi}\|_{L^2}(t)$, defined by

$$\|\phi - \overline{\phi}\|_{L^2}(t) = \sqrt{\int_{\mathbb{T}^2} (\phi(\boldsymbol{x}, t) - \overline{\phi}(t))^2\, \mathrm{d}\boldsymbol{x}}, \tag{2.17}$$

where

$$\overline{\phi}(t) = \int_{\mathbb{T}^2} \phi(\boldsymbol{x}, t)\, \mathrm{d}\boldsymbol{x}. \tag{2.18}$$

Note that the mix-norm and the scalar variance share the same time exponential scaling.

In systems with diffusion there is no particular advantage in using the mix-norm as an indicator of the degree of mixedness with respect to other more classical indicators, such as the variance of the concentration field $\|\phi - \overline{\phi}\|_{L^2}(t)$. However, when both advective-diffusive and purely advective systems are considered, the mix-norm provides, to the best of our knowledge, the sole global indicator of mixedness grounded on physical principles, which is able to quantify on equal footing the mixedness of these two systems. The reader interested in the general definition and physical interpretation of this measure of mixing is referred to the work by Mathew *et al.* (2005).

The mix-norm of the scalar field $\phi(\boldsymbol{x}, t)$ can be computed as follows (Mathew *et al.* 2005)

$$\mu_\phi(t) = \left[\sum_{\boldsymbol{k}\in\mathbb{Z}^2} \frac{1}{\sqrt{1+4\pi^2\|\boldsymbol{k}\|^2}} |\Phi_{\boldsymbol{k}}(t)|^2\right]^{1/2}, \tag{2.19}$$

where $\Phi_{\boldsymbol{k}}$ are the Fourier coefficients of the concentration field ϕ. Note that in the above expression less and less weight is given to the high-frequency harmonics. Hence the objective of an efficient mixing protocol is to shift, as quickly as possible, the frequency representation of any given initial scalar field to higher and higher frequencies.

The computation of the time evolution of the mix-norm is carried out using different algorithms in purely advecting and advecting–diffusing flows. On the one hand, in the case of finite diffusivity, the spectral representation of the scalar field (2.3) is evolved in time by (2.4) and (2.5). Hence, the mix-norm can be directly computed by substituting the Fourier coefficients $\Phi_{\boldsymbol{k}}$ of the concentration field into (2.19). On the other hand, in the diffusionless case, the mix-norm at the end of each switching time τ is obtained by computing the Fourier coefficients $\Phi_{\boldsymbol{k}}$ of the scalar field $\phi(x, y, k\tau)$, $k = 1, 2, \ldots, N$, by means of a Fast Fourier Transform (FFT), and substituting them into (2.19). In the numerical implementation of this algorithm, we discretized the domain at time $t = k\tau$, $k = 1, 2, \ldots, N$, with a grid of size 2048×2048 and constructed the concentration field $\phi(x, y, k\tau)$ using equation (2.13) and the map (2.14). The size of the grid has been chosen sufficiently large to ensure that the computed values of the mix-norm are independent of the grid size.

2.5. *Complexity of the optimization problem*

For a given value of the final optimization time T and a switching time τ, the set of admissible protocols corresponds to all the possible strings $\{\alpha_k\}_{k=1,2,\ldots,N}$ (with $N = T/\tau$), where α_k can assume any of the two symbols '0' and '1'. The set of all admissible protocols possesses the structure of a binary tree, and therefore its cardinality is equal to 2^N. Leveraging the homeomorphism

$$\mathscr{H}(x) = \sum_{k=1}^{\infty} \alpha_k / 2^k \tag{2.20}$$

between the real interval [0, 1] and the strings made by the sequences $\{\alpha_k\}_{k=1,2,\ldots,N}$ plus an infinite sequence of '0s', we can establish a bi-univocal correspondence between a set of stirring protocols $\{\alpha_k\}_{k=1,2,\ldots,N}$ and a set of rational numbers $x_\alpha = \sum_{k=1}^{N} \alpha_k/2^k$. This correspondence allows us to represent the protocols with a finite ordered set of rational points in the interval [0, 1]. In this representation the point $x_\alpha = 0$ corresponds to the protocol given by the steady flow $\boldsymbol{v}_0$ at any time $0 \leqslant t \leqslant T$, whereas the point $x_\alpha = \sum_{k=1}^{N} 1/2^k$, closest to the right extreme of the interval, corresponds to the protocol given by the steady flow $\boldsymbol{v}_1$ at any time $0 \leqslant t \leqslant T$. Furthermore, if $\boldsymbol{\alpha}^{(1)} = \{\alpha_1^{(1)}, \alpha_2^{(1)}, \ldots, \alpha_N^{(1)}\}$ and $\boldsymbol{\alpha}^{(2)} = \{\alpha_1^{(2)}, \alpha_2^{(2)}, \ldots, \alpha_N^{(2)}\}$ are any given pair of protocols, then the distance function

$$\mathrm{d}\big(\boldsymbol{\alpha}^{(1)}, \boldsymbol{\alpha}^{(2)}\big) = \sum_{k=1}^{N} \big|\alpha_k^{(1)} - \alpha_k^{(2)}\big| / 2^k \tag{2.21}$$

establishes a well-defined metric on this set of points (Devaney 1989). Hence, representative points that are close to each other are associated with protocols

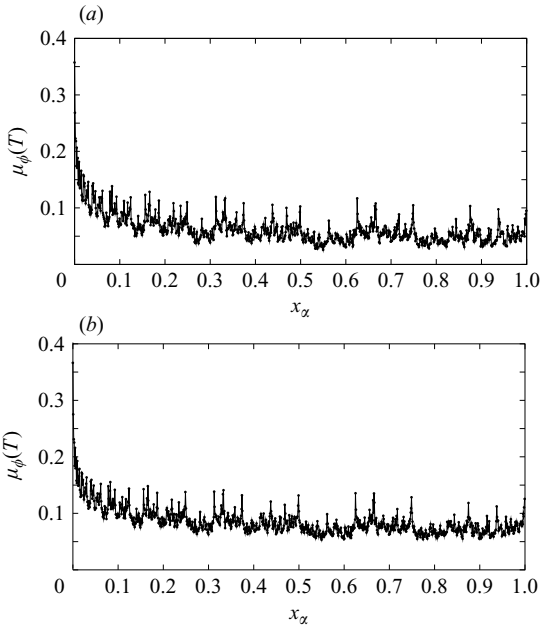

FIGURE 1. Mix-norm values μ_ϕ at a final time $T=4$ associated with the 2^{10} admissible protocols operating with switching time $\tau=0.4$. (*a*) Pure advection case ($Pe=\infty$), (*b*) advection–diffusion case at $Pe=10^4$.

which share a large portion of the sequence. This representation allows us to visualize the complexity of the optimization problem.

The optimal protocol is defined as the protocol, among all admissible protocols, which minimizes the mix-norm at final time T. Figure 1 shows the values of the mix-norm at the final time $T=4$, for all the admissible protocols with switching time $\tau=0.4$ for (*a*) the pure advection problem, and (*b*) the advection–diffusion problem at $Pe=10^4$, respectively. In both cases, the initial condition for the scalar field ϕ is

$$\phi(x,y,0)=\begin{cases} 1 & \text{for} \quad 0\leqslant x<1/2, \qquad 0\leqslant y<1, \\ -1 & \text{for} \quad 1/2\leqslant x<1, \qquad 0\leqslant y<1, \end{cases} \tag{2.22}$$

which represents a completely segregated initial mixture. Throughout this article, we exclusively use the above $\phi(x,y,0)$ as the initial condition for the optimization problem.

It is evident from figure 1 that the cost function possesses a complex structure of local minima both in (*a*) purely advective and (*b*) advective–diffusive flows. This complex structure makes common optimization strategies unsuitable for this specific problem. However, it is also evident from figure 1 that there are several local minima with values of the mix-norm nearly equal to the value associated with the absolute minimum of the cost function. The question we asked ourselves is the following: Is it worth searching for the absolute minimum, i.e. for the optimal protocol? Our answer to this question is no. The optimization procedure to find the optimal protocol is bound to be computationally expensive, and the mixing efficiency of the optimal protocol is bound to be nearly as good as the mixing efficiency of a sub-optimal protocol. Since the goal of this study is to provide an optimization procedure for

engineering applications, we propose finding a sub-optimal protocol with a sequence of short-time-horizon optimizations, which are computationally efficient.

3. Optimization strategy and results

3.1. *Optimization strategy*

Given a final optimization time T, a switching time $\tau = T/N$ and an integer ν, a sub-multiple of N, we define the optimization time horizon as $\tau\nu$. The parameter ν, the switching time horizon, represents the number of switching times needed to reach the horizon, while the parameter $m = N/\nu$ represents the total number of optimizations to be performed to reach the final time T. The definition of time horizon as the product of the parameters τ and ν is necessary because τ and ν play two different roles in the optimization strategy.

In order to make the optimization procedure physically meaningful, we define the time horizon in terms of the characteristic convective time T_K of the system. We define as very short and short time optimization horizons the horizons for which $0.1T_K \leqslant \nu\tau \leqslant 0.2T_K$ and $0.2T_K < \nu\tau \leqslant 0.4T_K$, respectively.

The meaning of terms 'very short' and 'short' is related to the mixing properties of the classical sine-flow, where the stirring protocol is purely periodic. A 'very short' time optimization horizon $\nu\tau$ is a time horizon for which the classical sine flow stirred by a periodic protocol with switching time equal to $\nu\tau$ gives rise to an almost integrable system, where the chaotic region occupies at most 10% of the domain (see e.g. figure 9*a* for the case $\nu\tau = 0.1$). A 'short' time optimization horizon $\nu\tau$ is a time horizon for which the classical sine flow gives rise to an almost globally chaotic system, where the chaotic region occupies at most 90% of the domain (see e.g. Figure 9(*b*) for the case $\nu\tau = 0.4$). Note that time optimization horizons $\nu\tau < 0.1T_K$ are not appealing for practical implementations of the optimization procedure because they imply a far-too-frequent analysis of the concentration field, which is computationally intensive. In other words, in engineering applications the computational time necessary to analyse the concentration field should be small compared with the time optimization horizon chosen.

Given a switching time τ and a switching time horizon ν, the optimization procedure is defined as follows. Starting at time $t = 0$, all of the 2^ν sub-protocols of the type $\{\alpha_1, \alpha_2, \ldots, \alpha_\nu\}$ are considered, and the solutions to the advection–diffusion or pure advection equations are computed in parallel for all these sub-protocols from the initial condition $\phi(x, y, 0)$ up to time $t = \nu\tau$. The mix-norm of each solution $\phi(x, y, \nu\tau)$ is then computed, and the protocol which produced the solution with the lowest mix-norm is selected. The procedure is repeated by considering the field $\phi(x, y, \nu\tau)$, generated by the best performing sub-protocol, as the initial condition for the next optimization up to time $t = 2\nu\tau$, and so on, until the final time $T = m\nu\tau = N\tau$ is reached. Therefore, for each choice of the parameters τ and ν, the above procedure selects a sub-optimal protocol out of $m2^\nu$ admissible protocols. We call this sub-optimal protocol a short-time-horizon optimal protocol. This optimization procedure does not find the optimal protocol by exploring exhaustively all the protocols admissible for a final optimization time T. On the contrary, it efficiently identifies a sub-optimal protocol by performing sequentially a direct examination of a very limited number of protocols at each time optimization horizon until the final optimization time T is reached.

We can estimate the computational cost of the above optimization procedure in terms of the total number N of possible switches of the velocity fields. There are 2^N

admissible protocols for a given final optimization time T and a switching time τ. An exhaustive analysis of all admissible protocols corresponds to the case where the time optimization horizon is chosen to be $T = N\tau$, i.e. $\nu = N$. This analysis implies the solution of 2^N advection–diffusion equations (2.2), or the advection equations (2.6), up to time $T = N\tau$. A measure of the computational cost is therefore the product of the number of admissible protocols times the interval of time over which the solution of equation (2.2), or (2.6), should be computed. It follows that the computational cost of an exhaustive optimization is $C_e = 2^N N\tau$, i.e. the cost grows exponentially with N. On the other hand, the proposed short-time-horizon optimization procedure implies the solution of only $N2^\nu/\nu$ advection–diffusion equations (2.2), or the advection equations (2.6), over a time horizon optimization equal to $\nu\tau$. Hence, the computational cost of the proposed short-time-horizon optimization is $C_s = 2^\nu N\tau$, i.e. the cost grows linearly with N. Obviously, the advantage of using the short time horizon optimization becomes exponentially more significant for higher values of N and smaller values of ν.

One of the scopes of this study is to analyse whether short-time-horizon optimal protocols can be designed and tested on purely advective flows and, subsequently, transported to advective-diffusive flows without a substantial deterioration of their mixing efficiency. In order to perform the proposed analysis, we need to introduce two types of optimizations: a kinematic-based optimization (KbOpt) and an advection–diffusion-based optimization (ADbOpt). The common goal of both optimizations is to select a short-time-horizon optimal protocol using the optimization procedure described above. The difference between KbOpt and ADbOpt lies in the type of equations solved while performing the optimization. On the one hand, for a given value of the switching time τ and the horizon ν, the KbOpt solves $N2^\nu/\nu$ pure advection equations (2.6) and selects a short-time-horizon optimal protocol $\boldsymbol{\alpha}_K(\tau, \nu)$. On the other hand, for a given value of τ, ν and Pe, the ADbOpt solves $N2^\nu/\nu$ advection–diffusion equations (2.2) and selects a short-time-horizon optimal protocol $\boldsymbol{\alpha}_D(\tau, \nu; Pe)$. In general the protocol $\boldsymbol{\alpha}_D(\tau, \nu; Pe)$ is different for different values of Pe, making the mixing optimization of advective–diffusive systems computationally expensive. Consequently, it is highly desirable to design and test a short-time-horizon optimal protocol $\boldsymbol{\alpha}_K(\tau, \nu)$ for a purely advective system and be able to apply it to the same system with diffusion, instead of deriving the more expensive protocols $\boldsymbol{\alpha}_D(\tau, \nu; Pe)$.

3.2. *Results*

In this section we present evidence of the feasibility, mixing efficiency and transportability of short-time-horizon optimal protocols for the specific mixing measure used in this study. The optimized protocols considered, $\boldsymbol{\alpha}_K(\tau, \nu)$ and $\boldsymbol{\alpha}_D(\tau, \nu; Pe)$, are those obtained via KbOpt and ADbOpt (at $Pe = 10^3$, 5×10^3, 10^4 and 5×10^4), respectively. We consider primarily these Péclet numbers, since in practical microflow applications the physical range of Pe values spans the interval $[10^2, 10^4]$ (Tabeling 2005). For example, if the characteristic velocity is $U = 0.1\,\mathrm{cm\,s^{-1}}$ and the characteristic length is $L = 0.01$ cm, then $Pe = 10^2$ corresponds to a diffusivity of about $10^{-5}\,\mathrm{cm^2\,s^{-1}}$, while $Pe = 10^4$ corresponds to a diffusivity of about $10^{-7}\,\mathrm{cm^2\,s^{-1}}$. Values of Pe higher than 5×10^4 are unrealistic in microflow systems.

In order to establish the mixing efficiency of the protocols $\boldsymbol{\alpha}_K(\tau, \nu)$ and $\boldsymbol{\alpha}_D(\tau, \nu; Pe)$, we compare their performance against the performance of the traditional sine flow protocol, a periodic protocol, defined by the alternating sequence $\boldsymbol{\alpha}_P(\tau) = \{0, 1, 0, 1, \ldots\}$. In addition, in order to establish the transportability of protocols $\boldsymbol{\alpha}_K(\tau, \nu)$ to flows with diffusivity, we compare their performance against the

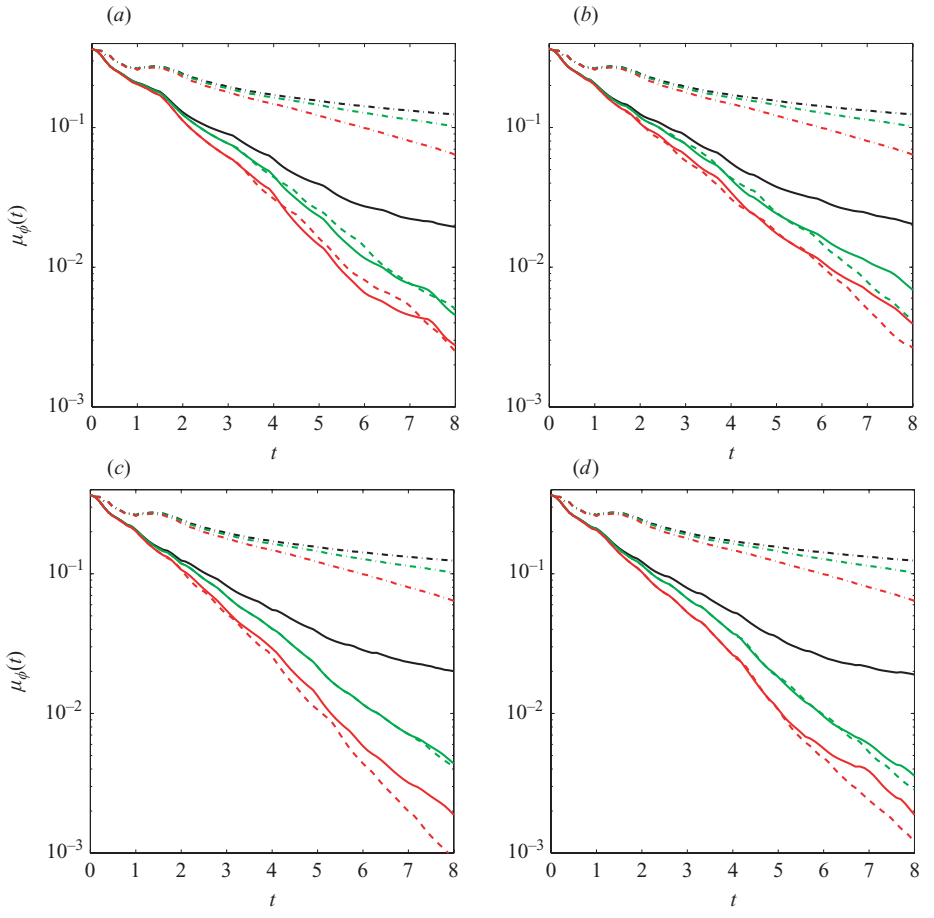

FIGURE 2. Time evolution of the mix-norm $\mu_\phi(t)$ induced by the protocols $\boldsymbol{\alpha}_P(\tau)$, $\boldsymbol{\alpha}_K(\tau, \nu)$ and $\boldsymbol{\alpha}_D(\tau, \nu; Pe)$ starting from the same initial condition. The protocols $\boldsymbol{\alpha}_K$ and $\boldsymbol{\alpha}_D$ have been optimized for the switching time $\tau = 0.1$ and different time switching horizons $\nu = 1$ (*a*), 2 (*b*), 4 (*c*), 8 (*d*). The line types identify the protocols: $\boldsymbol{\alpha}_P$ (dash-dotted), $\boldsymbol{\alpha}_K$ (solid) and $\boldsymbol{\alpha}_D$ (dashed). The colours identify the value of Pe: $Pe = 10^4$ (red), $Pe = 5 \times 10^4$ (green) and $Pe = \infty$ (black).

performance of the protocols $\boldsymbol{\alpha}_D(\tau, \nu; Pe)$ when both are applied to the sine flow with the same Pe values.

We restrict our study to the final time $T = 8$, and choose as switching times $\tau = 0.1$, 0.4 and 0.8 because, for these switching times, the periodic protocol $\boldsymbol{\alpha}_P(\tau)$ induces three well-defined flow structures by the final time T. For the switching time $\tau = 0.1$, the flow is dominated by two islands of regular motion, which occupy the entire flow domain: see figure 9(*a*). For the switching time $\tau = 0.4$, the flow is partially mixed. In this case, four islands of regular motion are surrounded by a chaotic region, which occupies about 90% of the flow domain: see figure 9(*b*). Finally, for $\tau = 0.8$, there are no detectable islands of regular motion, as the chaotic region invades the entire flow domain. Thus, a lower impact of the protocol optimization is expected in the latter case.

For the switching time $\tau = 0.1$, figure 2 shows the time evolution of the mix-norm induced by the protocols optimized for $\nu = 1, 2, 4, 8$, which correspond to time horizons

$0.1T_K$, $0.2T_K$, $0.4T_K$ and $0.8T_K$, respectively. The black, green and red dash-dotted curves show the mixing efficiency of the traditional periodic sine-flow protocol $\boldsymbol{\alpha}_P(\tau)$ for the purely advective case and the advective-diffusive cases at $Pe = 10^4$ and $Pe = 5 \times 10^4$, respectively. The results for the periodic protocol $\boldsymbol{\alpha}_P(\tau)$ are used as a reference to assess the mixing efficiency of the optimized protocols. The black solid line shows the mixing efficiency of the protocol $\boldsymbol{\alpha}_K(\tau, \nu)$, obtained using KbOpt, when applied to the purely advective case, $Pe = \infty$. This result is used as a reference to assess the transportability of the protocol $\boldsymbol{\alpha}_K(\tau, \nu)$ from purely advective to advective–diffusive flows. The green and red solid lines show the mixing efficiency of the protocol $\boldsymbol{\alpha}_K(\tau, \nu)$ when applied to the advective–diffusive cases at $Pe = 10^4$ and $Pe = 5 \times 10^4$, respectively. Finally, the green and red dashed lines show the mixing efficiency of the protocols $\boldsymbol{\alpha}_D(\tau, \nu; Pe)$, obtained using ADbOpt, at $Pe = 10^4$ and $Pe = 5 \times 10^4$, respectively.

Surprisingly, all protocols $\boldsymbol{\alpha}_K(\tau, \nu)$, optimized for $\nu = 1, 2, 4, 8$, induce nearly the same time evolution of the mix-norm in the diffusionless case ($Pe = \infty$), as shown in figures 2(*a*)–2(*d*) by the black solid lines. Hence, in the diffusionless case, very short-time-horizon optimal protocols ($\nu = 1, 2$) are indeed feasible and as efficient as the protocols optimized over longer time horizons. By comparing the black solid and dash-dotted lines in figures 2(*a*)–2(*d*), it is clear that the optimized protocols $\boldsymbol{\alpha}_K(\tau, \nu)$ (black solid line) are substantially more mixing-efficient than the periodic protocol $\boldsymbol{\alpha}_P(\tau)$ (black dash-dotted) over the entire length of the simulation. In particular, at final time T, the values of the mix-norm induced by the optimized protocols $\boldsymbol{\alpha}_K(\tau, \nu)$ are about a factor $1/6$ smaller than the value induced by the periodic protocol $\boldsymbol{\alpha}_P(\tau)$.

All the protocols $\boldsymbol{\alpha}_D(\tau, \nu; Pe)$ are remarkably more mixing efficient than the periodic protocol $\boldsymbol{\alpha}_P(\tau)$ for both values of Pe considered. Furthermore, the mixing efficiency of the protocols $\boldsymbol{\alpha}_D(\tau, \nu; Pe)$ with respect to the protocol $\boldsymbol{\alpha}_P(\tau)$, at corresponding Pe values, is substantially better than the mixing efficiency of the protocol $\boldsymbol{\alpha}_K(\tau, \nu)$ with respect to the protocol $\boldsymbol{\alpha}_P(\tau)$ at $Pe = \infty$. Contrary to the purely advective case, in the advective–diffusive case the mixing efficiency depends on the optimization horizon selected. At $Pe = 5 \times 10^4$, the most mixing-efficient is the protocol optimized over the longest switching time horizon considered, $\nu = 8$. In this case, at final time T, the value of the mix-norm induced by the optimized protocols $\boldsymbol{\alpha}_D(\tau, \nu; Pe)$ (green dashed line) is about a factor $1/33$ smaller than the value induced by the periodic protocol $\boldsymbol{\alpha}_P(\tau)$ (green dash-dotted line). Quite surprisingly, at $Pe = 10^4$, the most mixing-efficient is the protocol optimized for $\nu = 4$. In this case, at final time T, the value of the mix-norm induced by the optimized protocol $\boldsymbol{\alpha}_D(\tau, \nu; Pe)$ (red dash line) is about a factor $1/75$ smaller than the value induced by the periodic protocol $\boldsymbol{\alpha}_P(\tau)$ (red dashed-dotted line).

We assess the transportability of the protocol $\boldsymbol{\alpha}_K(\tau, \nu)$ from purely advective to advective–diffusive flows in two steps. We first compare the green and red solid lines with the black solid lines in figures 2(*a*)–2(*d*). In all cases the mixing efficiency of the protocol $\boldsymbol{\alpha}_K(\tau, \nu)$ improves substantially in the presence of diffusion with respect to the mixing efficiency of the same protocol in the absence of diffusion. Secondly, for the case $Pe = 5 \times 10^4$, we compare the green solid and dashed lines and, for the case $Pe = 10^4$, we compare the red solid and dashed lines. In general, the protocols $\boldsymbol{\alpha}_K(\tau, \nu)$ perform very well for all horizons and diffusivities even with respect to the protocols $\boldsymbol{\alpha}_D(\tau, \nu; Pe)$. Quite surprisingly, for the shortest switching time horizon, $\nu = 1$, the protocol $\boldsymbol{\alpha}_K(\tau, \nu)$, obtained using KbOpt, performs even better than the protocols $\boldsymbol{\alpha}_D(\tau, \nu; Pe)$ optimized using ADbOpt at $Pe = 10^4$ and 5×10^4, respectively. The best performance, however, is obtained for the switching time horizon $\nu = 8$, where the value of the mix-norm induced by the protocol $\boldsymbol{\alpha}_K(\tau, \nu)$ at $Pe = 5 \times 10^4$

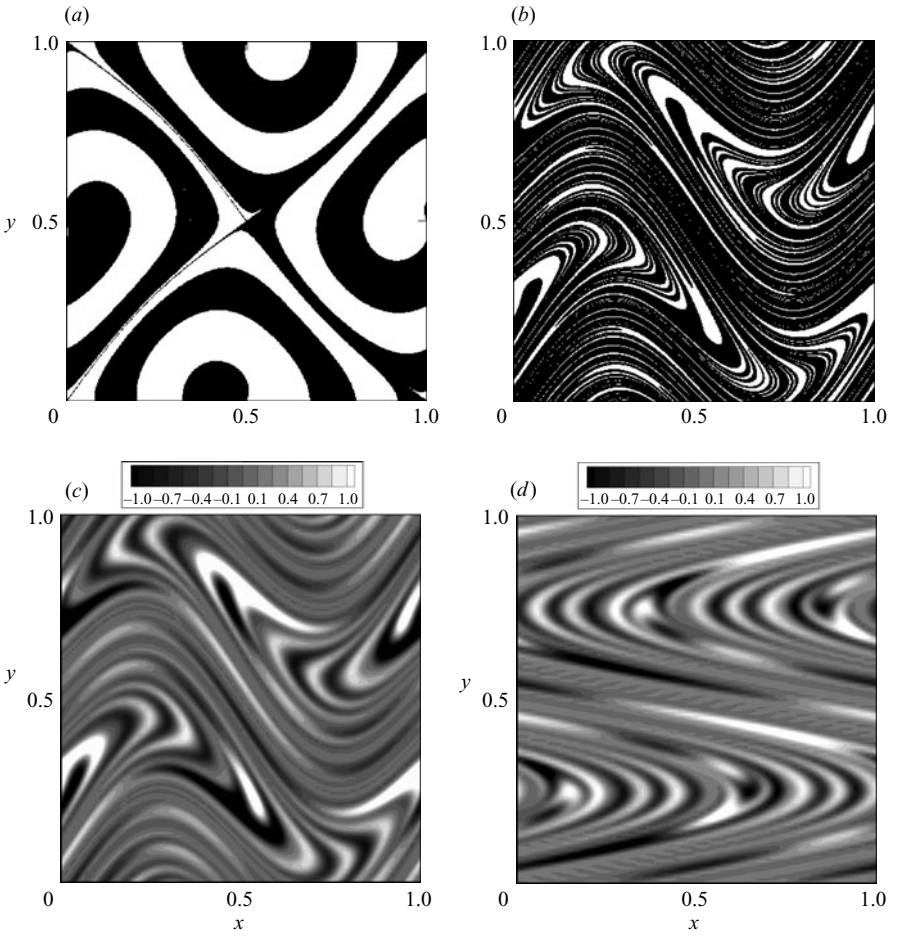

FIGURE 3. Snapshots at time $t = 4$ of the concentration field ϕ stirred by the protocols $\boldsymbol{\alpha}_P(\tau)$ at $Pe = \infty$ (*a*), $\boldsymbol{\alpha}_K(\tau, \nu)$ at $Pe = \infty$ (*b*), $\boldsymbol{\alpha}_K(\tau, \nu)$ at $Pe = 10^4$ (*c*), and $\boldsymbol{\alpha}_D(\tau, \nu; Pe)$ at $Pe = 10^4$ (*d*). The protocols $\boldsymbol{\alpha}_K(\tau, \nu)$ and $\boldsymbol{\alpha}_D(\tau, \nu; Pe)$ have been optimized for switching time $\tau = 0.1$ and switching time horizon $\nu = 1$.

(green solid line) is about a factor 1/28 smaller than the value induced by the periodic protocol $\boldsymbol{\alpha}_P(\tau)$ (green dash-dotted line), while the value of the mix-norm induced by the protocol $\boldsymbol{\alpha}_K(\tau, \nu)$ at $Pe = 10^4$ (red solid line) is about a factor 1/30 smaller than the value induced by the periodic protocol $\boldsymbol{\alpha}_P(\tau)$ (red dash-dotted line).

It is interesting to relate the value of the mix-norm to the geometry of the partially mixed concentration field. Figure 3(*a*) shows the snapshot at time $t = 4$ of the structure of the concentration field generated by the periodic protocol $\boldsymbol{\alpha}_P(\tau)$ in the diffusionless case; the corresponding value of the mix-norm can be read from the black dash-dotted line in figure 2(*a*). The stirring action of $\boldsymbol{\alpha}_P(\tau)$ induces the formation of swirl structures in correspondence of the two large islands of regular motion which occupy the entire flow domain. The characteristic size of the *lamellae* is of order one-tenth of the characteristic length L. Figure 3(*b*) shows the snapshot at time $t = 4$ of the structure of the concentration field generated by the protocol $\boldsymbol{\alpha}_K(\tau, \nu)$, optimized for $\tau = 0.1$ and $\nu = 1$, in the diffusionless case. The corresponding value of the mix-norm can be read from the black solid line in figure 2(*a*). The comparison between figures 3(*a*)

and 3(*b*) indicates that the protocol $\boldsymbol{\alpha}_K(\tau, \nu)$, obtained using KbOpt, is substantially more mixing-efficient than the periodic protocol $\boldsymbol{\alpha}_P(\tau)$ because its stirring action is able to induce much finer lamellar structures. Furthermore, the comparison of the two concentration fields highlights the different deformation mechanisms which characterize mixing in the regions of regular motion with respect to the chaotic region. Specifically, the spiralling structure generated by the periodic protocol $\boldsymbol{\alpha}_P(\tau)$ suggests that the overall effect of advection within the islands of regular motion closely mimics the advection field induced by a vortex. Instead, the filamented structure generated by the protocol $\boldsymbol{\alpha}_K(\tau, \nu)$ arises as a consequence of the recursive stretching and folding of the advected concentration field. Under the optimized stretching and folding, the average thickness of the lamellae decreases exponentially in time.

Figure 3(*c*) shows the snapshot at time $t = 4$ of the structure of the concentration field generated by the protocol $\boldsymbol{\alpha}_K(\tau, \nu)$, obtained using KbOpt, in the presence of diffusion ($Pe = 10^4$); the corresponding value of the mix-norm can be read from the red solid line in figure 2(*a*). The comparison between figures 3(*b*) and 3(*c*) shows the effect of molecular diffusion on the structure of the concentration field. Molecular diffusion is most effective in regions where the average thickness of the lamellae is of the same order of magnitude as the characteristic diffusion length. In these regions the concentration field is perfectly mixed. Everywhere else, instead, the effect of molecular diffusion results in a blurred structure with respect to the structure of the purely advective case.

Figure 3(*d*) shows the snapshot at time $t = 4$ of the structure of the concentration field generated by the protocol $\boldsymbol{\alpha}_D(\tau, \nu; Pe)$ optimized at $Pe = 10^4$, for $\tau = 0.1$ and $\nu = 1$, using ADbOpt. The corresponding value of the mix-norm can be read from the red dashed curve in figure 2(*a*). The spatial structure of the concentration field generated by the protocol $\boldsymbol{\alpha}_D(\tau, \nu; Pe)$ is, not surprisingly, different from the spatial structure produced by the protocol $\boldsymbol{\alpha}_K(\tau, \nu)$ applied to the same diffusive case, because the two protocols are different. Yet surprisingly, the performance of both protocols is very similar. The range of values of the concentration field, detectable as black and white intensities in figures 3(*c*) and 3(*d*), and the average striation thickness appear to be very similar, as indicated by the close values of the mix-norm in the two cases (see figure 2*a*, red solid and dashed lines).

For the switching time $\tau = 0.4$, figure 4 shows the time evolution of the mix-norm induced by the protocols optimized for $\nu = 1, 2, 4$, which correspond to time horizons $0.4T_K$, $0.8T_K$, $1.6T_K$, respectively. The line types and colours used in figure 4 represent the same quantities as in figure 2.

First of all, note that the mixing efficiency of the traditional periodic sine flow protocol $\boldsymbol{\alpha}_P(\tau)$ for the purely advective case and the advective–diffusive cases at $Pe = 10^4$ and $Pe = 5 \times 10^4$ (black, green and red dash-dotted lines, respectively) shows a modest improvement with respect to the case with switching time $\tau = 0.1$ (figure 2). This is a consequence of the fact that at switching time $\tau = 0.4$ (see figure 9*b*), the protocol $\boldsymbol{\alpha}_P(\tau)$ induces a partially mixed flow, where the overall mixing efficiency depends on how the chaotic region mediates the transport between the regions of regular motion (Cerbelli *et al.* 2004).

Consistently with the previous case ($\tau = 0.1$), all protocols $\boldsymbol{\alpha}_K(\tau, \nu)$, optimized for $\nu = 1, 2, 4$, induce nearly the same time evolution of the mix-norm in the diffusionless case ($Pe = \infty$), as shown in figures 4(*a*)–4(*c*) by the black solid lines. This result confirms that, in the diffusionless case, short-time-horizon optimal protocols ($\nu = 1$, 2) are indeed feasible and as efficient as the protocol optimized over the longer time horizon ($\nu = 4$). At final time T, the values of the mix-norm induced by the optimized

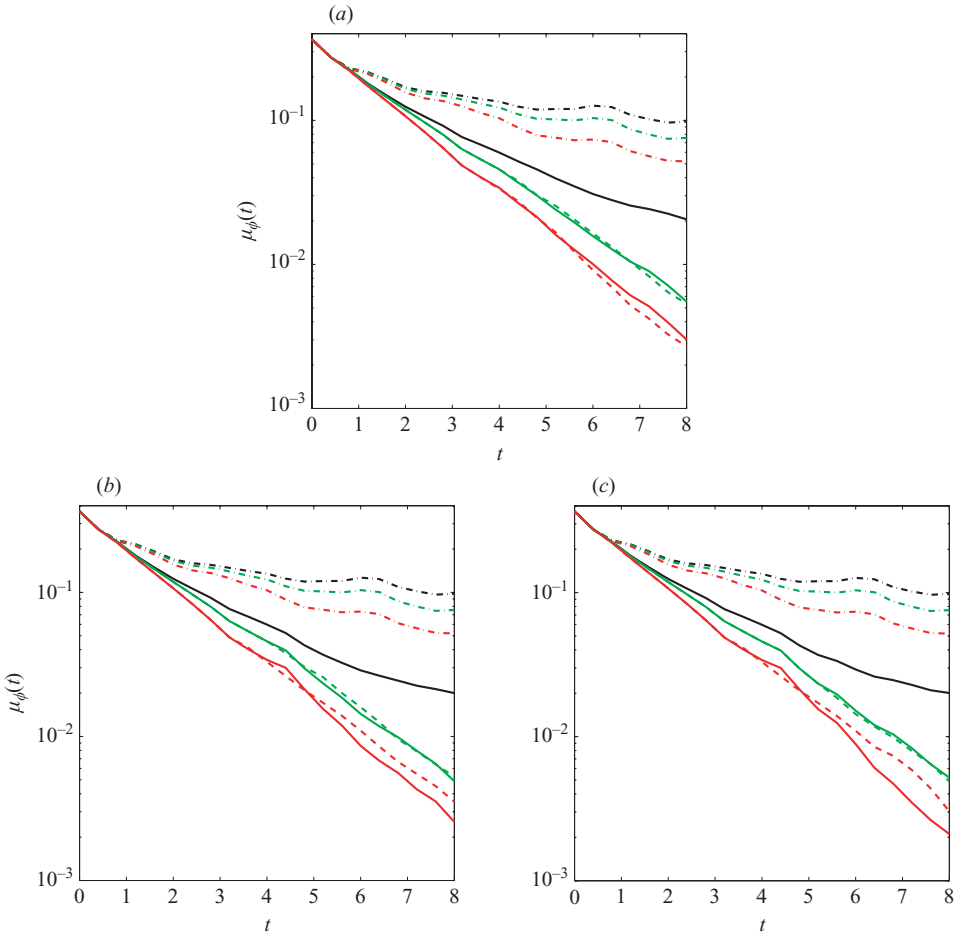

FIGURE 4. Time evolution of the mix-norm $\mu_\phi(t)$ induced by the protocols $\boldsymbol{\alpha}_P(\tau)$, $\boldsymbol{\alpha}_K(\tau, \nu)$ and $\boldsymbol{\alpha}_D(\tau, \nu; Pe)$ starting from the same initial condition. The protocols $\boldsymbol{\alpha}_K$ and $\boldsymbol{\alpha}_D$ have been optimized for the switching time $\tau = 0.4$ and different time switching horizons $\nu = 1(a)$, $2(b)$, $4(c)$. The line types identify the protocols: $\boldsymbol{\alpha}_P$ (dash-dotted), $\boldsymbol{\alpha}_K$ (solid) and $\boldsymbol{\alpha}_D$ (dashed). The colours identify the value of Pe: $Pe = 10^4$ (red), $Pe = 5 \times 10^4$ (green) and $Pe = \infty$ (black).

protocols $\boldsymbol{\alpha}_K(\tau, \nu)$ are about a factor $1/5$ smaller than the value induced by the periodic protocol $\boldsymbol{\alpha}_P(\tau)$ (compare the black solid and dash-dotted lines in figures 4*a*–4*c*).

Again, consistently with the previous case ($\tau = 0.1$), all the protocols $\boldsymbol{\alpha}_D(\tau, \nu; Pe)$ (green and red dashed lines) are remarkably more mixing-efficient than the periodic protocol $\boldsymbol{\alpha}_P(\tau)$ (green and red dash-dotted lines) for both values of Pe considered. Contrary to the previous case ($\tau = 0.1$), however, all protocols $\boldsymbol{\alpha}_D(\tau, \nu; Pe)$ present nearly the same mixing efficiency at both Pe values. At $Pe = 5 \times 10^4$, the protocol optimized for $\nu = 4$ is slightly more mixing-efficient than the other protocols. In this case, at final time T, the value of the mix-norm induced by the optimized protocol $\boldsymbol{\alpha}_D(\tau, \nu; Pe)$ (green dashed line) is about a factor $1/15$ smaller than the value induced by the periodic protocol $\boldsymbol{\alpha}_P(\tau)$ (green dash-dotted line). Instead, at $Pe = 10^4$, the protocol optimized for $\nu = 1$ is slightly more mixing-efficient than the other protocols. In this case, at final time T, the value of the mix-norm induced by the optimized

protocol $\boldsymbol{\alpha}_D(\tau, \nu; Pe)$ (red dashed line) is about a factor $1/17$ smaller than the value induced by the periodic protocol $\boldsymbol{\alpha}_P(\tau)$ (red dash-dotted line).

As before, we assess the transportability of the protocol $\boldsymbol{\alpha}_K(\tau, \nu)$ from purely advective to advective–diffusive flows in two steps. We first compare the red and green solid lines with the black solid lines in figures 4(*a*)–4(*c*). Consistently with the previous case ($\tau = 0.1$), the mixing efficiency of the protocol $\boldsymbol{\alpha}_K(\tau, \nu)$ improves substantially in the presence of diffusion. Secondly, for the case $Pe = 5 \times 10^4$, we compare the green solid lines with the green dashed lines. In this case the mixing efficiency of the protocol $\boldsymbol{\alpha}_K(\tau, \nu)$ is nearly the same as the efficiency of the protocol $\boldsymbol{\alpha}_D(\tau, \nu; Pe)$ optimized at $Pe = 5 \times 10^4$. For the case $Pe = 10^4$, we compare the red solid lines with the red dashed lines. In this case the mixing efficiency of the protocols $\boldsymbol{\alpha}_K(\tau, \nu)$ increases with increasing ν with respect to the efficiency of the protocols $\boldsymbol{\alpha}_D(\tau, \nu; Pe)$. In particular, for $\nu = 4$, at final time T, the value of the mix-norm induced by the protocol $\boldsymbol{\alpha}_K(\tau, \nu)$ (red solid line) is the lowest, about a factor $1/25$ smaller than the value induced by the periodic protocol $\boldsymbol{\alpha}_P(\tau)$ (red dash-dotted line). These results confirm that the protocols optimized using KbOpt can be effectively applied to flows with small molecular diffusivity.

The effect of the optimization on mixing efficiency is again better understood through the analysis of the geometrical structure of the mixture. Figure 5(*a*) shows the snapshot at time $t = 4$ of the structure of the concentration field generated by the periodic protocol $\boldsymbol{\alpha}_P(\tau)$ in the diffusionless case; the corresponding value of the mix-norm can be read from the black dash-dotted line in figure 4(*a*). The stirring action of $\boldsymbol{\alpha}_P(\tau)$ induces the formation of a partially mixed concentration field in which four unmixed regions, two white and two black, can be easily identified. These regions correspond to the islands of regular motion generated by the periodic protocol $\boldsymbol{\alpha}_P(\tau)$: see figure 9(*b*). These unmixed regions are surrounded by a mixture with much finer lamellar structure than the lamellar structure induced by the protocol $\boldsymbol{\alpha}_P(\tau)$ at switching time $\tau = 0.1$: see figure 3(*a*). The difference between the geometrical structure of the mixtures at switching time $\tau = 0.1$ and $\tau = 0.4$ is responsible for the difference in the corresponding mix-norm values.

Figure 5(*b*) shows the snapshot at time $t = 4$ of the structure of the concentration field generated by the protocol $\boldsymbol{\alpha}_K(\tau, \nu)$, optimized for $\tau = 0.4$ and $\nu = 1$, in the diffusionless case. The corresponding value of the mix-norm can be read from the black solid line in figure 4(*a*). The comparison between figures 5(*a*) and 5(*b*) indicates that the protocol $\boldsymbol{\alpha}_K(\tau, \nu)$, obtained using KbOpt, has been able to produce a more homogeneous mixture by inducing a recursive stretching and folding of the concentration field over the entire domain. Note that the protocol $\boldsymbol{\alpha}_K(\tau, \nu)$ at switching time $\tau = 0.4$ (figure 5*b*) is slightly less efficient than the protocol $\boldsymbol{\alpha}_K(\tau, \nu)$ at switching time $\tau = 0.1$ (figure 3*b*), as indicated by a slightly higher value of the mix-norm.

Figure 5(*c*) shows the snapshot at time $t = 4$ of the structure of the concentration field generated by the protocol $\boldsymbol{\alpha}_K(\tau, \nu)$, obtained using KbOpt, in the presence of diffusion ($Pe = 10^4$); the corresponding value of the mix-norm can be read from the red solid line in figure 4(*a*). The comparison between figures 5(*b*) and 5(*c*) shows the effect of molecular diffusion on the structure of the concentration field. As before, the effect of molecular diffusion is to blur the geometrical structures present in the purely advective case.

Figure 5(*d*) shows the snapshot at time $t = 4$ of the structure of the concentration field generated by the protocol $\boldsymbol{\alpha}_D(\tau, \nu; Pe)$, obtained using ADbOpt at $Pe = 10^4$; the corresponding value of the mix-norm can be read from the red dashed line in figure 4(*a*). Since the protocols $\boldsymbol{\alpha}_D(\tau, \nu; Pe)$ and $\boldsymbol{\alpha}_K(\tau, \nu)$ are different, the spatial

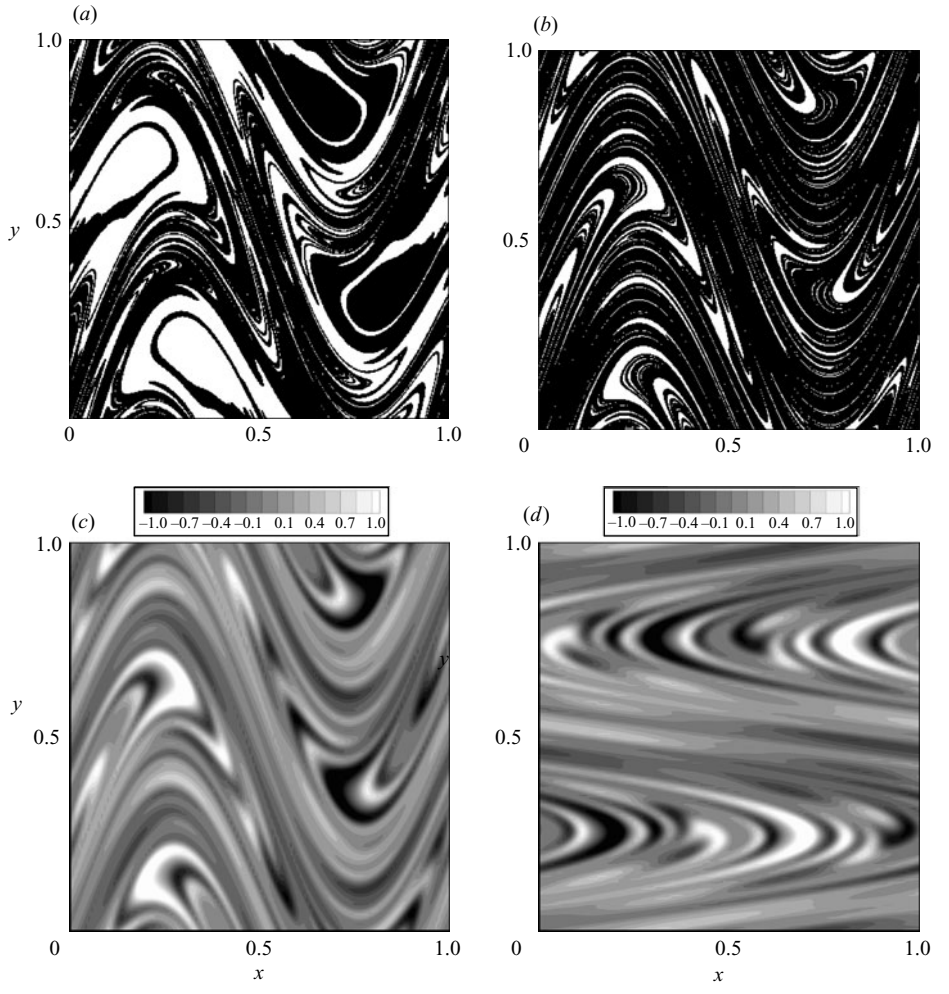

FIGURE 5. Snapshots at time $t = 4$ of the concentration field ϕ stirred by the protocols $\boldsymbol{\alpha}_P(\tau)$ at $Pe = \infty$ (*a*), $\boldsymbol{\alpha}_K(\tau, \nu)$ at $Pe = \infty$ (*b*), $\boldsymbol{\alpha}_K(\tau, \nu)$ at $Pe = 10^4$ (*c*), and $\boldsymbol{\alpha}_D(\tau, \nu; Pe)$ at $Pe = 10^4$ (*d*). The protocols $\boldsymbol{\alpha}_K(\tau, \nu)$ and $\boldsymbol{\alpha}_D(\tau, \nu; Pe)$ have been optimized for switching time $\tau = 0.4$ and switching time horizon $\nu = 1$.

structures they induce are also different. However, as before, the performance of both protocols is nearly the same. The range of values of the concentration field, detectable as black and white intensities in figure 5(*c*) and 5(*d*), and the average striation thickness appear very similar, as indicated by the close values of the mix-norm in the two cases (see figure 4*a*).

For switching time $\tau = 0.8$, figure 6 shows the time evolution of the mix-norm induced by the protocols optimized for $\nu = 1$, 2, which correspond to time horizons 0.8 T_K and 1.6 T_K, respectively. The line types and colours used in figure 6 represent the same quantities as in figure 2, but for the advection–diffusion case we show only the results related to the case $Pe = 10^4$.

The switching time $\tau = 0.8$ represents a challenge for the optimized protocols because, for this switching time, the traditional periodic sine flow protocol $\boldsymbol{\alpha}_P(\tau)$ induces a globally chaotic flow. This property reflects positively on the mixing

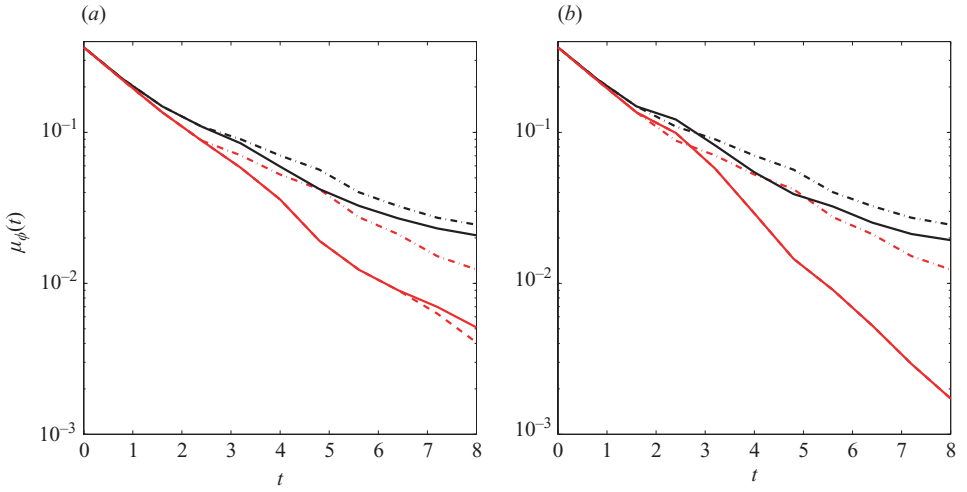

FIGURE 6. Time evolution of the mix-norm $\mu_\phi(t)$ induced by the protocols $\boldsymbol{\alpha}_P(\tau)$, $\boldsymbol{\alpha}_K(\tau, \nu)$ and $\boldsymbol{\alpha}_D(\tau, \nu; Pe)$ starting from the same initial condition. The protocols $\boldsymbol{\alpha}_K$ and $\boldsymbol{\alpha}_D$ have been optimized for the switching time $\tau = 0.8$ and different time switching horizons $\nu = 1(a)$, $2(b)$. The line types identify the protocols: $\boldsymbol{\alpha}_P$ (dash-dotted), $\boldsymbol{\alpha}_K$ (solid) and $\boldsymbol{\alpha}_D$ (dashed). The colours identify the value of Pe: $Pe = 10^4$ (red) and $Pe = \infty$ (black).

efficiency of the protocol $\boldsymbol{\alpha}_P(\tau)$ in the purely advective case and advective–diffusive case at $Pe = 10^4$ (black and red dash-dotted lines), respectively. In fact, the time evolution of the mix-norm shows a remarkable improvement of the mixing efficiency of $\boldsymbol{\alpha}_P(\tau)$ with respect to the cases with switching times $\tau = 0.1$ and 0.4.

Consistently with the previous cases ($\tau = 0.1$, 0.4), all protocols $\boldsymbol{\alpha}_K(\tau, \nu)$, optimized for $\nu = 1$, 2, induce nearly the same time evolution of the mix-norm in the diffusionless case ($Pe = \infty$), as shown in figures 6(a)–6(b) by the black solid lines. It is remarkable that, in the diffusionless case, these protocols have a better mixing efficiency of the globally chaotic periodic protocol $\boldsymbol{\alpha}_P(\tau)$ (black dash-dotted lines). This result clearly confirms that, in the diffusionless case, short-time-horizon optimal protocols ($\nu = 1$) are indeed feasible and as efficient as the protocol optimized over the longer time horizon ($\nu = 2$).

The mixing efficiency of the $\boldsymbol{\alpha}_D(\tau, \nu; Pe)$ optimized at $Pe = 10^4$ (red dashed lines in figures 6a–6b) further confirms that the short-horizon optimal protocols are more efficient than the globally chaotic periodic protocol $\boldsymbol{\alpha}_P(\tau)$ (red dash-dotted lines in figures 6a–6b).

Transportability in this case can be easily verified. In fact the protocols $\boldsymbol{\alpha}_K(\tau, \nu)$ and $\boldsymbol{\alpha}_D(\tau, \nu; Pe)$ share the first eight segments in the case $\nu = 1$ and are identical in the case $\nu = 2$ (compare red solid and dashed lines in figures 6a–6b).

3.3. *Robustness and applicability of the results*

Two were the main results presented in the previous subsection. The first result is the substantial mixing efficiency of short-time-horizon optimal protocols with respect to periodic protocols. Especially remarkable is the mixing efficiency of the protocols optimized for very short time horizons, e.g. $\tau = 0.1$, $\nu = 1, 2$. The second result is the robust transportability of short-time-horizon optimal protocols, designed for purely advective flows using KbOpt, to flows with small diffusivity, i.e. $Pe \geqslant 10^4$.

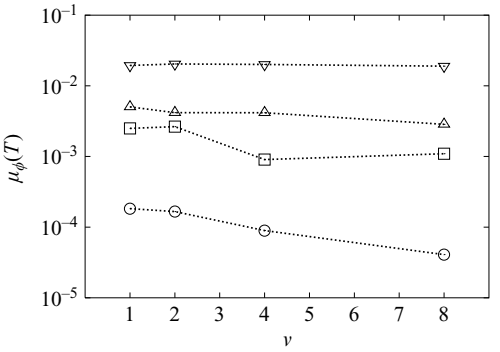

FIGURE 7. Values of the mix-norm $\mu_\phi(T)$ at the final time T produced by the protocol $\boldsymbol{\alpha}_D(\tau, \nu; Pe)$ optimized using ADbOpt for $\tau = 0.1$, $\nu = 1, 2, 4, 8$, and $Pe = 10^3$ ($\circ$), 10^4 ($\square$), 5×10^4 ($\triangle$), ∞ ($\triangledown$).

In order to assess conclusively the feasibility and mixing efficiency of very short-time-horizon optimal mixing protocols, it is important to characterize the effects of the choice of the switching time horizon ν and switching time τ on the outcome of the optimization procedure. The assessment can be accomplished in two steps: first, by analysing a representative set of cases generated by holding the time horizon $\tau\nu$ fixed while varying the switching time τ; second, by analysing a representative set of cases generated by holding the switching τ fixed while varying the switching time horizon ν.

Figure 4 shows, quite surprisingly, that the mixing enhancement obtained for switching time $\tau = 0.4$ by the optimized protocols $\boldsymbol{\alpha}_K(\tau, \nu)$ and $\boldsymbol{\alpha}_D(\tau, \nu; Pe)$ with respect the periodic protocol $\boldsymbol{\alpha}_P(\tau)$ is, for all the Pe values, less pronounced than the corresponding enhancement obtained for switching time $\tau = 0.1$ (see figure 2). To explain this seemingly counter-intuitive result we compare figure 4(a) with figure 2(c), which have the same time horizon $0.4T_K$, and figure 4(b) with figure 2(d), which have the same time horizon $0.8T_K$. For the purely advective case, the black solid curves show that the mixing efficiency of the protocol $\boldsymbol{\alpha}_K(\tau, \nu)$, optimized for $\tau = 0.1$ and $\nu = 4$, 8, is slightly better than the efficiency of the protocol $\boldsymbol{\alpha}_K(\tau, \nu)$ optimized for $\tau = 0.4$ and $\nu = 1$, 2. For the advective-diffusive case, the green and red dashed curves show that the mixing efficiency of the protocol $\boldsymbol{\alpha}_D(\tau, \nu; Pe)$ optimized for $\tau = 0.1$ and $\nu = 4$, 8 is definitively better than the efficiency of the protocol $\boldsymbol{\alpha}_D(\tau, \nu; Pe)$ optimized for $\tau = 0.4$ and $\nu = 1, 2$ for both values of diffusivity. Since the only difference between the two sets of data is the number of times the velocity field has been switched within a given time horizon, this comparison indicates that, for a given horizon, it is better to optimize a protocol choosing a switching time which is a sub-multiple of the time horizon.

Figure 7 shows the values of the mix-norm induced by the protocol $\boldsymbol{\alpha}_D(\tau, \nu; Pe)$ optimized for $\tau = 0.1$, $\nu = 1, 2, 4, 8$, and $Pe = 10^3$ ($\circ$), 10^4 ($\square$), 5×10^4 ($\triangle$), ∞ ($\triangledown$) (the dotted linear interpolants have been added to facilitate the interpretation of the plot). On the one hand, the curves show that as Pe decreases, the protocols $\boldsymbol{\alpha}_D(\tau, \nu; Pe)$ optimized over longer switching time horizons present the best mixing efficiency. On the other hand, the curves show that the improvement in mixing efficiency is not substantial and decreases as Pe increases. In other words, the protocols $\boldsymbol{\alpha}_D(\tau, \nu; Pe)$ optimized over very short switching time horizons are feasible and competitively efficient with respect to protocols optimized over longer time horizons and, consequently, appealing for on-line optimization of mixing processes.

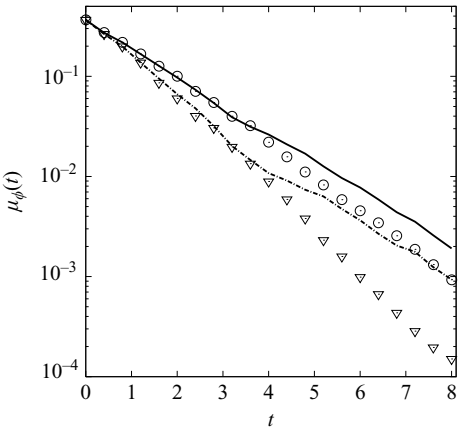

FIGURE 8. Time evolution of the mix-norm $\mu_\phi(t)$ produced by the protocols $\boldsymbol{\alpha}_K(\tau, \nu)$ and $\boldsymbol{\alpha}_D(\tau, \nu; Pe)$ optimized for the switching time horizon $\nu = 1$ and switching time $\tau = 0.4$. Solid line: protocol $\boldsymbol{\alpha}_K(\tau, \nu)$, $Pe = 5 \times 10^3$; Dash-dotted line: protocol $\boldsymbol{\alpha}_K(\tau, \nu)$, $Pe = 10^3$; $\circ$, protocol $\boldsymbol{\alpha}_D(\tau, \nu; Pe)$, $Pe = 5 \times 10^3$; $\triangledown$; protocol $\boldsymbol{\alpha}_D(\tau, \nu; Pe)$, $Pe = 10^3$.

The transportability of the protocols $\boldsymbol{\alpha}_K(\tau, \nu)$, optimized using KbOpt, to diffusive systems is bound to deteriorate as molecular diffusion increases, i.e. as Pe decreases. In particular, for $Pe < 10^4$, protocols derived using KbOpt and ADbOpt could produce significantly different results. For example, figure 8 shows the time evolution of the mix-norm induced by these two types of protocols when optimized for $\nu = 1$ and $\tau = 0.4$. The solid and dash-dotted lines show the mixing efficiency of the protocol $\boldsymbol{\alpha}_K(\tau, \nu)$, obtained using KbOpt, when applied to the advective–diffusive cases at $Pe = 10^3$ and $Pe = 5 \times 10^3$, respectively. The triangles ($\triangledown$) and circles ($\circ$) show the mixing efficiency of the protocols $\boldsymbol{\alpha}_D(\tau, \nu; Pe)$, obtained using ADbOpt, at $Pe = 10^3$ and $Pe = 5 \times 10^3$, respectively. At both Pe values, the trend of the mixing efficiency of the protocols $\boldsymbol{\alpha}_K(\tau, \nu)$ and $\boldsymbol{\alpha}_D(\tau, \nu; Pe)$ is similar. Over short time scales ($t \leqslant 2$), the mixing efficiency of the protocols $\boldsymbol{\alpha}_K(\tau, \nu)$ and $\boldsymbol{\alpha}_D(\tau, \nu; Pe)$ is practically identical, even at such relatively small Pe values of the order of 10^3. This is not surprising, since the early stages of a mixing process are essentially controlled by advection (Giona *et al.* 2002). However, for $t > 3$, the mixing efficiency of the protocols $\boldsymbol{\alpha}_D(\tau, \nu; Pe)$ improves substantially with respect to the mixing efficiency of the protocols $\boldsymbol{\alpha}_K(\tau, \nu)$. Note, however, that the difference between the mixing efficiencies of the protocols obtained using KbOpt and ADbOpt decreases monotonically as Pe increases. We should conclude that the transportability of the protocols obtained using KbOpt becomes less robust at values of Pe between $Pe = 5 \times 10^3$ and $Pe = 10^4$. For $Pe \leqslant 5 \times 10^3$, on-line optimization over very short time horizons could still be implemented, at a higher computational cost, directly using the ADbOpt procedure.

The robustness of the results presented indicates that the short-time-horizon optimization technique presented in this article could be used to optimize mixing devices in which mixing is achieved through the switching of two or more steady flows, such as in cavity flows or in electrokinetic mixers. The method proposed could be implemented both *off-line* and *on-line*. The *off-line* implementation, the simplest, can be used to improve any mixing device for which the stirring velocity field can be closely approximated by blinking a set of steady state solutions to the Navier–Stokes equations. In this case, the short-time-horizon optimization follows

literally the procedure presented in this article for the sine flow. The result of the *off-line* optimization is a sub-optimal protocol which can be applied to the mixing device for better performance. The *on-line* implementation of the short-time-horizon optimization should take place during the evolution of the mixing process itself. This case is limited by the practical feasibility of measuring on-line the pointwise state of a mixture, i.e. the concentration of the advecting–diffusing scalar field. This practical problem is not peculiar to the short-time-horizon optimization, but it is shared by any method aimed at optimizing mixing performance simultaneously with the evolution of the mixing process itself.

4. Properties of the optimized protocols

In this section, we provide an interpretation of the results obtained so far in terms of the asymptotic properties of the optimized protocols, both in the pure advection and in the advection–diffusion cases. In particular, we quantify the mixing efficiency of the optimized protocols using the Lyapunov exponents and Poincaré sections for the pure advection case and the eigenvalue–eigenfunction spectra for the advection–diffusion case.

In order to recast the short-time-horizon mixing problem within a setting suitable for asymptotic analysis, we introduce the periodic continued protocols $\pi_K(\tau, \nu)$ and $\pi_D(\tau, \nu; Pe)$ of the optimized protocols $\boldsymbol{\alpha}_K(\tau, \nu)$ and $\boldsymbol{\alpha}_D(\tau, \nu; Pe)$, respectively. The periodic continued protocols $\pi_K(\tau, \nu)$ and $\pi_D(\tau, \nu; Pe)$ are defined as the time-periodic protocols of period T obtained by repeating the sequences $\boldsymbol{\alpha}_K(\tau, \nu)$ and $\boldsymbol{\alpha}_D(\tau, \nu; Pe)$ an infinite number of times, respectively. For completeness of notation, we also define in the same terms the periodic continuation $\pi_P(\tau)$ of the periodic protocol $\boldsymbol{\alpha}_P(\tau)$.

4.1. *Kinematic analysis*

We recall that a Poincaré section is obtained by superimposing onto the same plot the positions at times $t = nT$, $n = 0, 1, 2, \ldots$, of a few initial conditions that evolve under the periodically continued protocols. Figures 9(*a*) and 9(*b*) depict the Poincaré section associated with the protocol $\pi_P(\tau = 0.1)$ and $\pi_P(\tau = 0.4)$, while figures 9(*c*) and 9(*d*) present the Poincaré section associated with the protocol $\pi_K(\tau, \nu)$ optimized for $\tau = 0.1$, $\nu = 1$ and $\tau = 0.4$, $\nu = 1$, respectively ($T = 8$ for all the computations). Figure 9(*a*) was obtained by selecting and evolving in time 18 initial conditions, spanning a parallel and a meridian of the torus, in order to characterize the structure of the regions of regular motion. In figures 9(*b*)–9(*d*), the chaotic region was obtained by selecting and evolving in time a single initial condition located near the midpoint of the square (1/2, 1/2). In figure 9(*b*), the four egg-shaped regions are islands of regular motion.

The Poincaré sections (figures 9*c* and 9*d*) associated with the protocols $\pi_K(\tau, \nu)$ show that the stirring action of the periodically continued protocols, obtained using KbOpt, generates flows that are globally chaotic. We verified that all the protocols considered in this study, obtained using ADbOpt or KbOpt, induce the same qualitative globally chaotic structure of the Poincaré sections as in figures 9(*c*) and 9(*d*).

While the Poincaré section provides a visually qualitative assessment of the dynamics induced by the stirring action of the protocols, a quantitative comparison between the mixing efficiency of the different protocols can be obtained by computing the Lyapunov exponent Λ_L. The exponent Λ_L is defined as the limit $\Lambda_L = \lim_{n\to\infty}(1/nT)\log(\|\boldsymbol{l}_n\|/|\boldsymbol{l}_0\|)$, where the vector $\boldsymbol{l}_n$ is the nth image of an initial

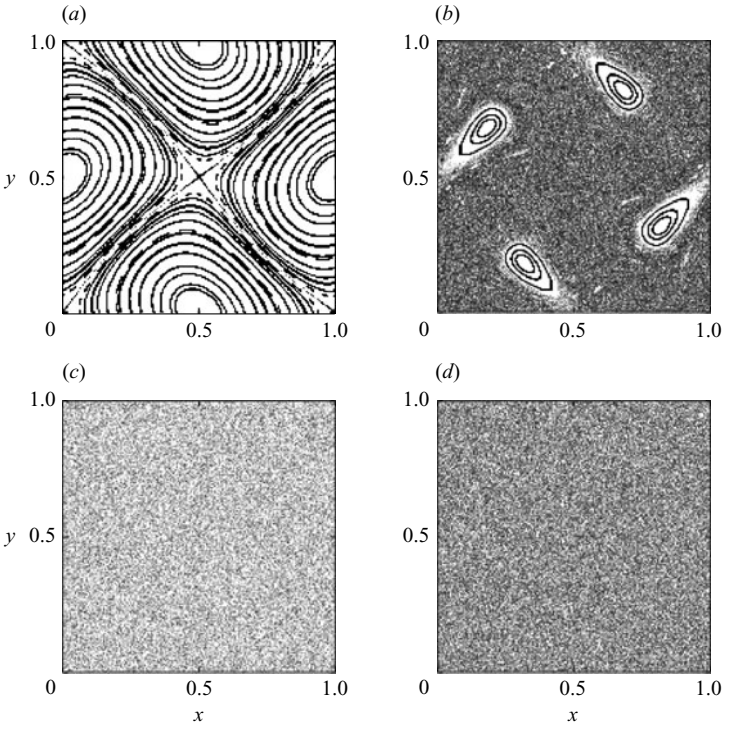

FIGURE 9. Poincaré sections of the periodically continued protocols: (*a*) $\pi_P(\tau = 0.1)$; (*b*) $\pi_P(\tau = 0.4)$; (*c*) $\pi_K(\tau = 0.1, \nu = 1)$; (*d*) $\pi_K(\tau = 0.4, \nu = 1)$.

vector $\boldsymbol{l}_0$ attached to a generic point of the chaotic region that evolves under the differential, i.e. the Jacobian matrix, of the Poincaré stroboscopic map.

Figure 10(*a*) shows the Lyapunov exponent for all the optimal protocols presented in this article with switching time $\tau = 0.4$. The data show that all of the optimized protocols have comparable values of Λ_L, the only exception being the protocol denoted by I, which represents the periodic case $\pi_P(\tau)$, therefore not optimized.

Figure 10(*b*) shows the inverse of the mix-norm at the final optimization time $T = 8$ for the same protocols shown in figure 10(*a*). The higher the value of $[\mu_\phi(T)]^{-1}$, the higher is the mixing efficiency of the associated protocol. Note how the periodic protocol, denoted I, is characterized by the lowest values of both the Lyapunov exponent and $[\mu_\phi(T)]^{-1}$.

The comparison of figures 10(*a*) and 10(*b*) indicates that the highest mixing efficiency in terms of mix-norm value at $T = 8$ does not coincide with the highest asymptotic value of the Lyapunov exponent of the periodically continued protocol. In other words, the existence of a globally chaotic condition, i.e. the existence of a Lebesgue ergodic trajectory characterized by a positive Lyapunov exponent, does not yield direct quantitative information about mixing efficiency at short times associated with an assigned protocol and a given initial condition. However, the information conveyed by the value of the Lyapunov exponent has important implications for the transportability of the protocols π_K. In fact, the existence of a globally chaotic condition qualitatively guarantees the successful transportability of the protocols $\boldsymbol{\alpha}_K(\tau, \nu)$, obtained using KbOpt, from purely advective to advective–diffusive flows with small molecular diffusivity.

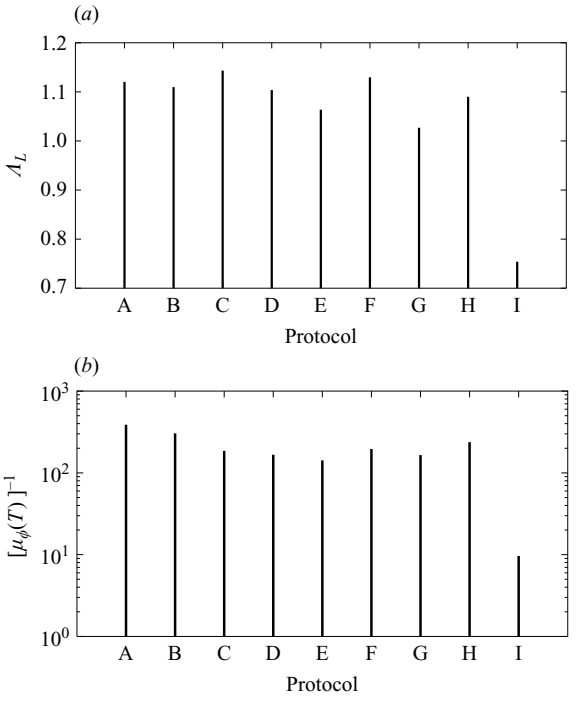

FIGURE 10. (*a*) Lyapunov exponent of periodically continued protocols optimized for different time switching horizons ν and fixed switching time $\tau = 0.4$. (*b*) Inverse value of the mix-norm, i.e. $[\mu_\phi(T)]^{-1}$, at time $T = 8$ for the same protocols as in panel (*a*). Labelling of the protocols is as follows: A, π_D associated with $\nu = 10$, $Pe = 10^4$; B, π_K with $\nu = 10$; C, π_D with $\nu = 1$, $Pe = 10^4$; D, π_K with $\nu = 1$; E, π_D with $\nu = 2$, $Pe = 10^4$; F, π_K with $\nu = 2$; G, π_D with $\nu = 4$, $Pe = 10^4$; H, π_K with $\nu = 4$; I, periodic protocol π_P.

4.2. *Homogenization properties of optimized protocols*

To complement the kinematic analysis presented in the previous subsection, we analyse the properties of the advection–diffusion operator associated with the periodic continuations $\pi_K(\tau, \nu)$ of short-time-horizon optimal protocols $\boldsymbol{\alpha}_K(\tau, \nu)$ obtained using KbOpt.

It can be shown that the mix-norm of the solution of the advection–diffusion equation driven by the protocol $\pi_K(\tau, \nu)$ displays an asymptotic exponential decay of the type

$$\mu_\phi(t) \sim \mathrm{e}^{-\Lambda_{hom} t}, \tag{4.1}$$

for any initial conditions possessing zero mean. Note that this is a property common to all time-periodic flow systems evolving in a closed and bounded domain, such as the sine flow considered in this study. Cerbelli *et al.* (2004) have shown that the characteristic decay exponent Λ_{hom} can be written in terms of the absolute value of the dominant eigenvalue λ_d of the Poincaré operator as follows: $\Lambda_{hom} = -\log|\lambda_d|/T$.†

† Note that the Poincaré operator associated with the advection–diffusion equation in closed systems possesses $\lambda = 1$ as the largest eigenvalue in absolute value. This eigenvalue is associated with the constant eigenfunction. The eigenvalue λ_d is, strictly speaking, the second eigenvalue in absolute value. However, it can be properly referred to as the dominant eigenvalue if one restricts the problem to the functional space of square summable functions possessing zero mean.

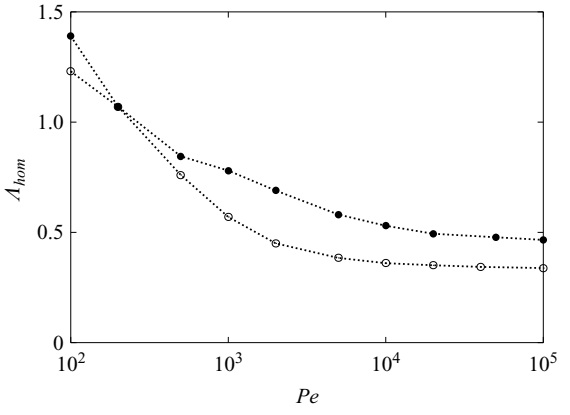

FIGURE 11. Characteristic decay exponent Λ_{hom}; ●, S-branch for the protocol $\pi_K(\tau, \nu)$ with $\tau = 0.4$ and $\nu = 2$; ○, S-branch for the strictly periodic protocol $\pi_P(\tau)$ with $\tau = 0.8$.

The characteristic decay exponent Λ_{hom} depends on the Péclet number. For high Péclet numbers, the scaling of Λ_{hom} versus Pe is an indicator of the type of interaction between the advection and diffusion mechanisms which sets up asymptotically. In other words, the values and the asymptotic scaling of the dominant eigenvalue Λ_{hom} provide important information about the mixing efficiency of the protocol and the chaotic condition of the system, respectively (Cerbelli *et al.* 2004; Giona *et al.* 2004*b*).

The spectrum of the eigenvalues of the Poincaré operator associated with the advection–diffusion equation driven by the protocol $\pi_K(\tau, \nu)$, or by the strictly periodic protocol $\pi_P(\tau)$, possesses two main spectral branches (Cerbelli *et al.* 2004). These branches are excited by initial conditions possessing a pure cosine (C-branch) or a pure sine (S-branch) Fourier expansion, respectively. Since the initial condition (2.22) considered throughout this article admits vanishing projection onto the C-branch of the spectrum, we consider only the S-branch. Consequently, this branch corresponds to the actual asymptotic decay rate of the concentration field obtained by stirring the initial condition (2.22) with a protocol $\pi_K(\tau, \nu)$.

In order to characterize the type of asymptotic dynamics induced by the protocols $\pi_K(\tau, \nu)$ when applied to the advection–diffusion equation, we analyse the power-law relationship between the characteristic decay exponent Λ_{hom} and the Péclet number Pe. The solid symbols in figure 11 show the behaviour of the characteristic decay exponent Λ_{hom} as a function of the Péclet number for the S-branch of the spectrum associated with the protocol $\pi_K(\tau, \nu)$ optimized for $\tau = 0.4$ and $\nu = 2$. For brevity, we analyse only this protocol, since the other optimized protocols discussed in the previous subsections yield to qualitative analogous results. The solid symbols in figure 11 show that $\Lambda_{hom} \sim Pe^0$ for large Pe values, which indicates that the system is in a globally chaotic condition for these large Pe values. This result further confirms that the protocols $\boldsymbol{\alpha}_K(\tau, \nu)$ induce, once periodically continued, a globally chaotic dynamics throughout the whole mixing space when applied to both purely advective or advective–diffusive flow systems. Furthermore, these results explain the robust transportability of the protocols $\boldsymbol{\alpha}_K(\tau, \nu)$ to flow systems with $Pe \geqslant 5 \times 10^3$.

In order to characterize the relaxation toward the homogeneous condition of the concentration field stirred by the protocol $\pi_K(\tau, \nu)$ when applied to the advection–diffusion equation, we compare the values of the characteristic decay exponent Λ_{hom} for the protocols $\pi_K(\tau, \nu)$ with the values of Λ_{hom} associated with the strictly periodic

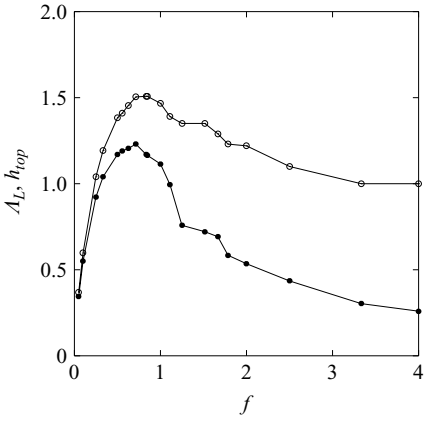

FIGURE 12. Lyapunov exponent Λ_L (●) and topological entropy h_{top} (○) versus the frequency $f = 1/2\tau$ associated with the family of strictly periodic protocols $\pi_P(\tau)$.

protocols $\pi_P(\tau = 0.8)$. We choose $\pi_P(\tau = 0.8)$ because a numerical analysis performed on the periodic protocols $\pi_P(\tau)$ for $\tau \in [0, 1]$ (Cerbelli *et al.* 2004) showed that, for $\tau = 0.8$, not only is the kinematics globally chaotic, but also the advection–diffusion equation driven by this protocol possesses the highest characteristic scaling exponent Λ_{hom} of all periodic protocols (see figure 11, open symbols).

The quantitative values of Λ_{hom} for $Pe \geqslant 5 \times 10^3$ characterize the relaxation of the concentration field, stirred by the protocols $\pi_K(\tau, \nu)$, toward homogeneous condition. Figure 11 shows that the optimized protocol π_K (solid symbols) yields, for $Pe > 10^4$, to values of $\Lambda_{hom} \simeq 0.44$, which are significantly greater than the values $\Lambda_{hom} \simeq 0.33$ produced by the strictly periodic protocol $\pi_P(\tau = 0.8)$ (open symbols). This result indicates that the optimized protocol π_K is significantly more mixing-efficient than the protocol π_P in the presence of diffusion for high Péclet numbers.

To summarize, the analysis of the homogenization properties of the short-time-horizon optimal protocol $\pi_K(\tau = 0.4, \nu = 2)$, obtained using KbOpt, indicates that such a protocol has a significantly better mixing efficiency and homogenization than periodic protocols. This is essentially a consequence of the fact that the optimal protocol π_K induces, once periodically continued, globally chaotic dynamics faster than the periodic protocols. These results are indeed very promising for practical engineering applications.

Throughout this subsection we have considered only protocols obtained using KbOpt, since the analysis of this case is more critical, because the role of diffusion, which is explicitly accounted for in the ADbOpt, is to enhance mixing. However, we have verified that analogous homogenization performance can be achieved by the protocols obtained using ADbOpt.

4.3. *Lyapunov exponents and power spectra of the optimized protocols*

We complete the characterization of the short-time-horizon optimal protocols by analysing and comparing the Lyapunov exponents and the frequency spectra of the protocols $\pi_K(\tau, \nu)$ with the Lyapunov exponents and the frequency spectra of the strictly periodic protocols $\pi_P(\tau)$.

Figure 12 shows the behaviour of the maximum Lyapunov exponent Λ_L (solid symbols) and the topological entropy h_{top} (open symbols) associated with the periodic protocols $\pi_P(\tau)$ versus the frequency $f = 1/2\tau$ of the stirring velocity field. In order

to provide a fair comparison between flows possessing different frequencies, the data depicted in figure 12 are the maximum Lyapunov exponents and the topological entropies multiplied by the frequency f of the stirring velocity field. The topological entropy provides the characteristic scaling exponent for the time evolution of the length $l(t)$ of a generic material line advected by the flow at time t, i.e. $l(t) \sim l(0)\mathrm{e}^{h_{top}t}$ (Katok & Hasselblatt 1995). By definition, the topological entropy is always greater than or at least equal to the Lyapunov exponent, i.e. $h_{top} \geqslant \Lambda_L$ for all frequencies.

The periodic protocol $\pi_P(\tau)$ with the best mixing efficiency is the one which produces the highest values of the maximum Lyapunov exponent and topological entropy. From figure 12, it is easy to see that the periodic protocol $\pi_P(\tau)$ with the best mixing performance is the one with frequency $f \simeq 0.625$ corresponding to a periodic protocol with switching time $\tau \simeq 0.8$. The stirring action of protocol $\pi_P(\tau = 0.8)$ has been shown to induce globally chaotic dynamics.

The results presented in figure 12 allow us to better understand why all protocols $\boldsymbol{\alpha}_K(\tau, \nu)$ presented in this article have a better mixing efficiency than the periodic protocols $\boldsymbol{\alpha}_P(\tau)$ (see figure 2 for $\tau = 0.1$, figure 4 for $\tau = 0.4$, and figure 6 for $\tau = 0.8$). In order to leverage the results given in figure 12, we need to perform a Fourier analysis in time of the optimal protocols $\boldsymbol{\alpha}_K(\tau, \nu)$. Given a flow protocol $\boldsymbol{\alpha}_K(\tau, \nu) = \{\alpha_1, \alpha_2, \ldots, \alpha_N\}$, we compute the Fourier series of the step impulse function $\alpha(t)$ associated with the sequence $\{\alpha_p\}_{p=1}^N$, i.e. $\alpha(t) = \alpha_p$ for $(p-1)\tau \leqslant t < p\tau$, $p = 1, \ldots, N$. Obviously, the impulse function for the protocol $\pi_K(\tau, \nu)$ is obtained by periodically continuing the impulse function $\alpha(t)$ associated with the protocol $\boldsymbol{\alpha}_K(\tau, \nu)$.

Figure 13 presents the impulse functions (a, c, e) and power spectra (b, d, f) associated with the periodic protocol $\boldsymbol{\alpha}_P(\tau = 0.8)$ (a, b), and with the protocols $\boldsymbol{\alpha}_K(\tau, \nu)$ optimized for the switching time horizon $\nu = 1$ and switching time $\tau = 0.4$ (c, d), and for $\nu = 2$ and $\tau = 0.4$ (e, f). Figure 13(b), which is used as a reference case, presents the power spectrum of the globally chaotic periodic protocol $\boldsymbol{\alpha}_P(\tau = 0.8)$. The spectrum is the typical spectrum of a square wave (see figure 13a) with a large spike at the fundamental frequency, $f = 0.625$, and smaller spikes at the odd harmonics. The two smaller spikes shown in figure 13(b) correspond to frequencies $f = 1.875$ and $f = 3.125$, respectively.

It is interesting to compare the spectra of the protocols $\boldsymbol{\alpha}_K(\tau = 0.4, \nu = 1)$ (figure 13d) and $\boldsymbol{\alpha}_K(\tau = 0.4, \nu = 2)$ (figure 13f) with the spectrum of the periodic protocol $\boldsymbol{\alpha}_P(\tau = 0.8)$ (figure 13b). The two spectra are very different. The spectrum of protocol $\boldsymbol{\alpha}_K(\tau = 0.4,\ \nu = 1)$ presents two broad peaks centred at frequencies $f = 0.45$ and 0.75, respectively. Unexpectedly, the spectrum goes to zero exactly at frequency $f = 0.625$. The spectrum of protocol $\boldsymbol{\alpha}_K(\tau = 0.4, \nu = 2)$, instead, presents a small peak at $f = 0.25$ and a dominant peak at $f = 0.625$. Since in the diffusionless case (compare figures 4 and 6) the mixing efficiencies of the protocols $\boldsymbol{\alpha}_K(\tau = 0.4, \nu = 1)$ and $\boldsymbol{\alpha}_K(\tau = 0.4, \nu = 2)$ are nearly identical and better than the mixing efficiency of the globally chaotic periodic protocol $\boldsymbol{\alpha}_P(\tau = 0.8)$, it follows that a protocol can be globally chaotic without having a spectrum with a dominant peak centred near the frequency $f = 0.625$. It is essential, instead, that the spectrum has highest-possible frequency content in the range $0.4 \leqslant f \leqslant 1.2$ where the Lyapunov exponent and topological entropy have their highest values.

It is not surprising that the optimization procedure selects as a short-time-horizon optimal protocol an aperiodic protocol: see figures 13(c) and 13(e). As noted by Liu *et al.* (1994*a*), aperiodic protocols do not present periodic points and, consequently, flows stirred by such protocols are free of islands of regular motion. However, given

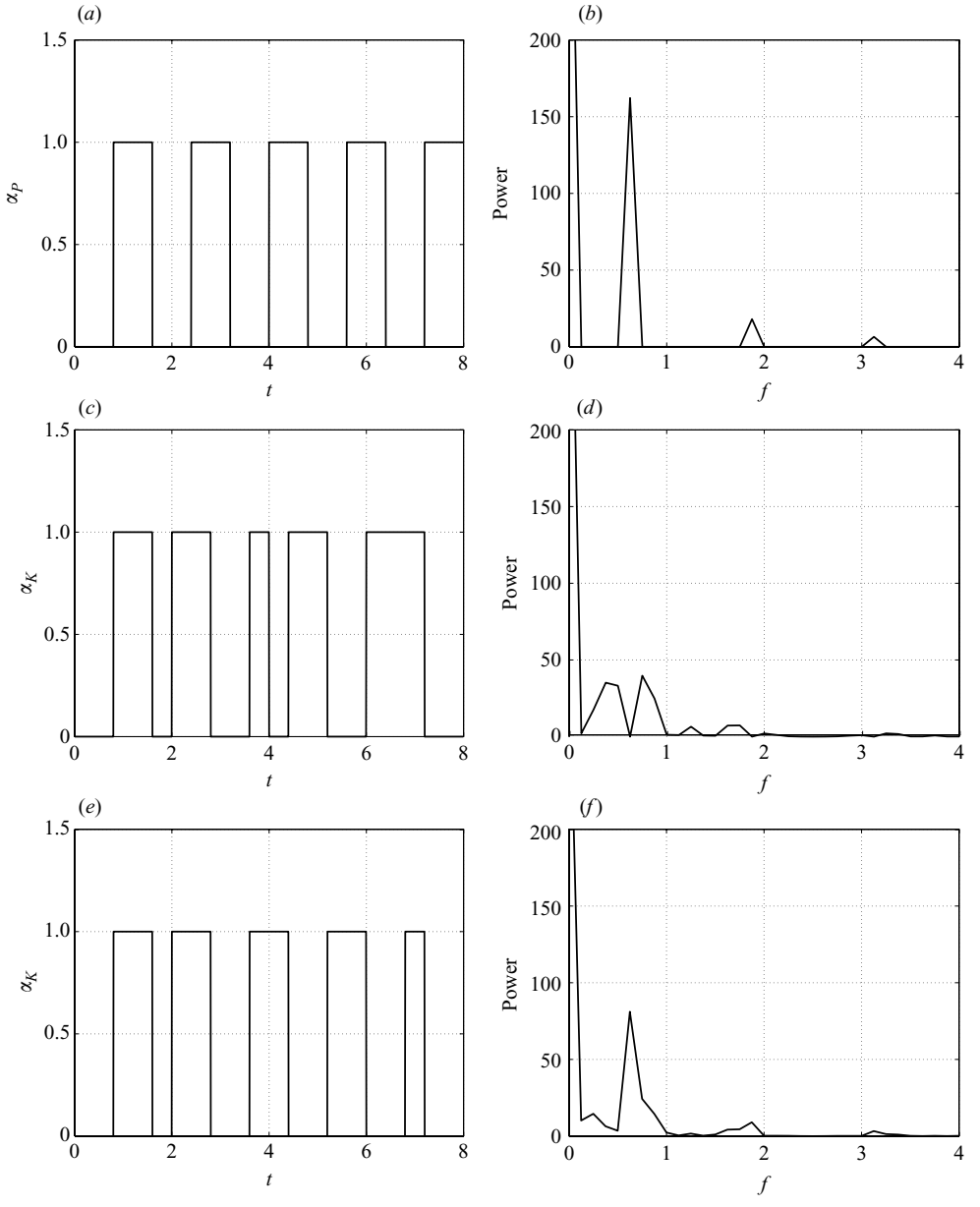

FIGURE 13. Impulse functions (a, c, e) and power spectra (b, d, f) associated with the periodic protocol $\boldsymbol{\alpha}_P(\tau = 0.8)$ (a, b), and with the protocols $\boldsymbol{\alpha}_K(\tau, \nu)$ optimized for the switching time horizon $\nu = 1$ and switching time $\tau = 0.4$ (c, d), and for $\nu = 2$ and $\tau = 0.4$ (e, f).

a final optimization time T and a switching time τ, there are 2^N admissible protocols ($N = T/\tau$), the large majority of which are aperiodic. Furthermore, as shown in figure 1, there is a large percentage of poorly efficient protocols, most of which are aperiodic. Hence, the outcome of the optimization procedure is not trivial. The sequence of optimizations narrows down the initial pool of 2^N admissible protocols to the best performing one: a highly efficient aperiodic protocol which has a high-frequency content in the range $0.4 \leqslant f \leqslant 1.2$.

The comparison between Lyapunov exponents, power spectrum and mixing efficiency of the short time optimal mixing protocols $\boldsymbol{\alpha}_K(\tau = 0.4, \nu = 1)$, $\boldsymbol{\alpha}_K(\tau = 0.4, \nu = 2)$ and the globally chaotic periodic protocol $\boldsymbol{\alpha}_P(\tau = 0.8)$, allow us to draw some important conclusions. The periodic protocol $\boldsymbol{\alpha}_P(\tau = 0.8)$ has the highest Lyapunov exponent, $\Lambda_L = 1.2$, of all protocols analysed in this study. Based on the value of the Lyapunov exponents, one could jump at the conclusion that the periodic protocol $\boldsymbol{\alpha}_P(\tau = 0.8)$ is the most mixing-efficient. However, figures 2, 4 and 6 clearly show that the periodic protocol $\boldsymbol{\alpha}_P(\tau = 0.8)$ has the worst mixing efficiency among all short-time-horizon optimal mixing protocols both in the pure advection and in the advection–diffusion cases. The difference in mixing efficiency is especially large when the protocols optimized using KbOpt are used to stir initially segregated mixture with small molecular diffusivity, i.e. $Pe \geqslant 10^4$. This is a further indication that even globally chaotic protocols possessing almost identical values of the maximum Lyapunov exponent may display substantially different mixing properties in the presence of diffusion for $Pe \to \infty$.

5. Conclusions

In this study, we considered the problem of deriving a computationally cost-effective optimization procedure able to generate feasible, mixing-efficient and transportable protocols. As a case study, we considered the optimization of mixing protocols for a two-dimensional, piecewise steady, nonlinear flow, the sine flow, in both purely advecting and advecting–diffusing cases. We used the mix-norm as the cost function to be minimized by the optimization procedure. The mix-norm is a scalar variance averaged over all the possible coarse graining of the flow domain, which provides an overall measure of mixing efficiency for flows with or without molecular diffusivity.

We showed that the cost function possesses a complex structure of local minima of nearly the same values and, consequently, that the problem possesses a large number of sub-optimal protocols with nearly the same mixing efficiency as the optimal protocol. Since the goal of this study is to provide an optimization procedure for engineering applications, we proposed finding a sub-optimal protocol with a sequence of short-time-horizon optimizations, which are computationally efficient. This approach consists of subdividing the overall optimization interval T in sub-intervals, or time horizons, and finding the optimal sub-protocol for each of these sub-intervals. The sequence of optimal sub-protocols generates a sub-optimal protocol, called the short-time-horizon optimal protocol, for the flow under consideration.

We compared the performance of the protocols $\boldsymbol{\alpha}_K(\tau, \nu)$ generated by the kinematic-based optimization (KbOpt), i.e. the protocols obtained by minimizing the mix-norm of the scalar field governed by the pure advection equation, with the performance of the protocols $\boldsymbol{\alpha}_D(\tau, \nu; Pe)$ generated by the advection–diffusion-based optimization (ADbOpt), i.e. the protocols obtained by minimizing the mix-norm of the scalar field governed by the advection–diffusion equation.

We presented evidence of the feasibility, mixing efficiency and transportability of short-time-horizon optimal protocols for the specific mixing measure used in this study. We established the mixing efficiency of the protocols $\boldsymbol{\alpha}_K(\tau, \nu)$ and $\boldsymbol{\alpha}_D(\tau, \nu; Pe)$, by comparing their performance against the performance of the traditional periodic sine flow protocol $\boldsymbol{\alpha}_P(\tau)$. We established the transportability of protocols $\boldsymbol{\alpha}_K(\tau, \nu)$ to flows with diffusivity, by comparing the time evolution of the mix-norm associated with the optimal protocols $\boldsymbol{\alpha}_D(\tau, \nu; Pe)$ and $\boldsymbol{\alpha}_K(\tau, \nu)$ for the same Pe values.

Two main results have been presented in this study. The first result is the substantial mixing efficiency of short-time-horizon optimal protocols with respect to periodic protocols. Especially remarkable is the mixing efficiency of the protocols optimized for very short time horizons, e.g. $\tau = 0.1,\ \nu = 1, 2$. The second result is the robust transportability of short-time-horizon optimal protocols, designed for purely advective flows using KbOpt, to flows with small diffusivity, i.e. $Pe \geqslant 10^4$.

We conclusively assessed the feasibility and mixing efficiency of very short-time-horizon optimal mixing protocols by characterizing the effects of the choice of the switching time horizon ν and switching time τ on the outcome of the optimization procedure. Protocols optimized over very short time horizons are feasible and competitively efficient with respect to protocols optimized over longer time horizons and, consequently, appealing for on-line optimization of mixing processes. However, for a given switching time horizon, it is better to optimize a protocol by choosing a switching time which is a sub-multiple of the time horizon.

We also assessed that the transportability of the protocols obtained using KbOpt is robust for $Pe \geqslant 10^4$. The transportability becomes less robust at values of Pe between $Pe = 5 \times 10^3$ and $Pe = 10^4$. Nevertheless, for $Pe \leqslant 5 \times 10^3$, optimization over very short time horizons could still be implemented, at a higher computational cost, directly using the ADbOpt procedure.

We provided an interpretation of our results in terms of the asymptotic properties of the optimized protocols both in the pure advection and in the advection–diffusion cases. In particular, we quantified the mixing efficiency of the periodically continued protocols using the Lyapunov exponents and Poincaré sections for the pure advection case and the eigenvalue–eigenfunction spectra for the advection–diffusion case.

In order to recast the short-time-horizon mixing problem within a setting suitable for asymptotic analysis, we introduced the concept of periodically continued protocols. The periodic continued protocols are defined as the time-periodic protocol of period T obtained by repeating the sequence $\boldsymbol{\alpha}_K(\tau, \nu)$ and $\boldsymbol{\alpha}_D(\tau, \nu; Pe)$ an infinite number of times, respectively.

Our analysis demonstrated that the highest mixing efficiency in terms of mix-norm value at the final optimization time does not coincide with the highest asymptotic value of the Lyapunov exponent of the periodically continued protocol. In other words, the existence of a globally chaotic condition, i.e. the existence of a Lebesgue ergodic trajectory characterized by a positive Lyapunov exponent, does not yield direct quantitative information about mixing efficiency at short times associated with an assigned protocol and a given initial condition.

We showed, however, that the information conveyed by the value of the Lyapunov exponent has important implications for the transportability of the protocols $\boldsymbol{\alpha}_K(\tau, \nu)$. In fact, the existence of a globally chaotic condition for the periodically continued protocol $\pi_K(\tau, \nu)$ qualitatively guarantees the successful transportability of the protocols $\boldsymbol{\alpha}_K(\tau, \nu)$, obtained using KbOpt, from purely advective to advective–diffusive flows with small molecular diffusivity.

The analysis of the homogenization properties of the short-time-horizon optimal protocols $\pi_K(\tau, \nu)$, obtained using KbOpt, indicated that such protocols have a significantly better mixing efficiency and homogenization than the strictly periodic protocols $\pi_P(\tau)$. We showed that this is essentially a consequence of the fact that the optimal protocol $\boldsymbol{\alpha}_K(\tau, \nu)$ induces, once periodically continued, a globally chaotic dynamics faster than the periodic protocols.

The analysis of the power spectra of protocols $\boldsymbol{\alpha}_K(\tau, \nu)$ showed that a protocol induces globally chaotic dynamics if its spectrum has the highest-possible frequency

content in the range $0.4 \leqslant f \leqslant 1.2$ where the Lyapunov exponent and topological entropy of the periodic protocols $\pi_P(\tau)$ have their highest values.

The results obtained in this study indicate that the optimization over very short time horizons could be used in principle as an on-line procedure for enhancing mixing in a laboratory experiment and, in the future, in engineering applications. Work is under way to extend our results to three-dimensional closed and open systems.

The authors wish to thank Dr Stefano Cerbelli for several valuable discussions pertaining to this research. This work has been partially supported by NSERC under grant RGPIN217169.

REFERENCES

Arnold, V. I. & Avez, A. 1989 *Ergodic Problems of Classical Mechanics*. Addison-Wesley.

Alvarez, M. M., Arratia, P. E. & Muzzio, F. J. 2002*a* Laminar mixing in eccentric stirred tank systems. *Can. J. Chem. Engng* **80**, 546–557.

Alvarez, M. M., Shinbrot, T., Zalc, J. & Muzzio, F. J. 2002*b* Practical chaotic mixing. *Chem. Engng Sci.* **17**, 3749–3753.

Balasuriya, S. 2005 Optimal perturbation for enhanced chaotic transport. *Physica* D **202**, 155–176.

Beigie, D., Leonard, A. & Wiggins, S. 1994 Invariant manifold templates for chaotic advection. *Chaos Solitons Fractals* **4**, 749–868.

Boyland, P. L., Aref, H. & Stremler, M. A. 2000 Topological fluid mechanics of stirring. *J. Fluid Mech.* **403**, 277–304.

Cerbelli, S., Vitacolonna, V., Adrover, A. & Giona, M. 2004 Eigenvalue–eigenfunction analysis of infinitely fast reactions and micromixing regimes in regular and chaotic bounded flows. *Chem. Engng Sci.* **59**, 2125–2144.

Devaney, R. 1989 *An Introduction to Chaotic Dynamical Systems*. 2nd edn. Perseus Books.

D'Alessandro, D., Dahleh, M. & Mezić, I. 1999 Control of mixing in fluid flow: A maximum entropy approach. *IEEE Trans. Aut. Contr.* **44**, 1852–1863.

Fountain, G. O., Khakhar, D. V. & Ottino, J. M. 1997 Visualization of three-dimensional chaos. *Science* **31**, 683–686.

Franjione, J. G. & Ottino, J. M. 1992 Symmetry concepts for geometric analysis of mixing flows. *Phil. Trans. R. Soc. Lond.* A **338**, 301–323.

Giona, M., Cerbelli, S. & Adrover, A. 2002 Geometry of reaction interfaces in chaotic flows. *Phys. Rev. Lett.* **88**, 024501 I–IV.

Giona, M., Cerbelli, S., & Vitacolonna, V. 2004*a* Universality and imaginary potentials in advection–diffusion equations in closed flows. *J. Fluid Mech.* **513**, 221–237.

Giona, M., Adrover, A., Cerbelli, S. & Vitacolonna, V. 2004*b* Spectral properties and transport mechanisms of partially chaotic bounded flows in the presence of diffusion. *Phys. Rev. Lett.* **92**, 114101 I–IV.

Harvey, III, A. D., Wood, S. P. & Leng, D. E. 1997 Experimental and computational study of multiple impeller flows. *Chem. Engng Sci.* **52**, 1479–1491.

Hobbs, D. M., & Muzzio, F. J. 1998 Optimization of a static mixer using dynamical systems techniques. *Chem. Engng Sci.* **53**, 3199–3213.

Hobbs, D. M., Alvarez, M. M. & Muzzio, F. J. 1997 Mixing in globally chaotic flows: A self-similar process. *Fractals* **5**, 395–425.

Katok, A. & Hasselblatt, B. 1995 *Introduction to the Modern Theory of Dynamical Systems*. Cambridge University Press.

Lamberto, D. J., Muzzio, F. J., Swanson, P. D. & Tonkovich, A. L 1996 Using time-dependent RPM to enhance mixing in stirred vessels. *Chem. Engng Sci.* **51**, 733–741.

Liu, W. & Haller, G. 2004 Inertial manifolds and completeness of eigenmodes for unsteady magnetic dynamos. *Physica* D **194**, 297–319.

Liu, M., Muzzio, F. J. & Peskin, R. L. 1994*a* Quantification of mixing in aperiodic chaotic flows. *Chaos Solitons Fractals* **4**, 869–893.

Liu, M., Peskin, R. L., Muzzio, F. J., & Leong, C. W. 1994*b* Structure of the stretching field in chaotic cavity flows. *AIChE J.* **40**, 1273–1286.

Mathew, C., Mezić, I., & Petzold, L. 2005 A multiscale measure for mixing. *Physica* D **211**, 23–46.

Mathew, C., Mezić, I., Grivopoulos, S., Vaidya, U. & Petzold, L. 2007 Optimal control of mixing in Stokes fluid flows. *J. Fluid Mech.* **580**, 261–281.

Metcalfe, G., Rudman, M., Brydon, A., Graham, L. J. W. & Hamilton, R. 2005 Composing chaos: An experimental and numerical study of an open duct mixing flow. *AIChE J.* **52**, 9–28.

Noack, B. R., Mezić, I., Tadmor, G. & Banaszuk, A. 2004 Optimal mixing in recirculation zones. *Phys. Fluids* **16**, 867–888.

Ottino, J. M. 1989 *The Kinematics of Mixing: Stretching, Chaos and Transport*. Cambridge University Press.

Ottino, J. M. & Wiggins, S. 2004*a* Designing optimal micromixers. *Science* **305**, 485–486.

Ottino, J. M. & Wiggins, S. 2004*b* Introduction: Mixing in microfluidics. *Phil. Trans. R. Soc. Lond.* A **362**, 923–935.

Rice, M., Hall, J., Papadakis, G. & Yanneskis, M. 2006 Investigation of laminar flow in a stirred vessel at low Reynolds numbers. *Chem. Engng Sci.* **61**, 2762–2770.

Rom-Kedar, V., Leonard, A. & Wiggins, S. 1990 An analytic study of transport, mixing and chaos in an unsteady vortical flow. *J. Fluid Mech.* **214**, 347–394.

Sharma, A. & Gupte, N. 1997 Control methods for problems of mixing and coherence in chaotic maps and flows. *Pramana J. Phys.* **488**, 231–248.

Stremler, M. A., Haselton, F. R. & Aref, H. 2004 Designing for chaos: Applications of chaotic advection at the microscale. *Phil. Trans. R. Soc. Lond.* A **362**, 1019–1036.

Tabeling, P. 2005 *Introduction to Microfluidics*. Oxford University Press.

Tabeling, P., Chabert, M., Dodge, A., Jullien, C. & Okkels, F. 2004 Chaotic mixing in cross-channel micromixer. *Phil. Trans. R. Soc. Lond.* **362**, 987–1000.

Tay, F. E. H. 2002 *Microfluidics and BioMEMS Applications*. Kluwer.

Thiffeault, J. L., Doering, C. R. & Gibbon, J. D. 2004 A bound on mixing efficiency for the advection–diffusion equation. *J. Fluid Mech.* **521**, 105–114.

Thiffeault, J.-L. & Finn, M. D. 2006 Topology, braids and mixing in fluids. *Phil. Trans. R. Soc. Lond.* A **364**, 3251–3266.

Toussaint, V., Carriere, P., & Raynal, F. 1995 A numerical Eulerian approach to mixing by chaotic advection. *Phys. Fluids* **7**, 2587–2600.

Toussaint, V., Carriere, P., Scott, J. & Gence, J. N. 2000 Spectral decay of a passive scalar in chaotic mixing. *Phys. Fluids* **12**, 2834–2844.

Vikhansky, A. 2002*a* Enhancement of laminar mixing by optimal control methods. *Chem. Engng Sci.* **57**, 2719–2725.

Vikhansky, A. 2002*b* Control of stretching rate in time-periodic chaotic flows. *Phys. Fluids* **14**, 2752–2756.

Wiggins, S. & Ottino, J. M. 2004 Foundations of chaotic mixing. *Phil. Trans. R. Soc. Lond.* A **362**, 937–970.

Wojtkowski, M. 1981 A model problem with the coexistence of stochastic and integrable behavior. *Commun. Math. Phys.* **80**, 453–464.

Xia, H. M., Shu, C., Wan, S. Y. M. & Chen, Y. T. 2006 Influence of the Reynolds number on chaotic mixing in a spatially periodic micromixer and its characterization using dynamical system techniques. *J. Micromech. Microengng* **16**, 53–61.

Zalc, J. M., Szalai, E. S. & Muzzio F. J. 2003 Mixing dynamics in the SMX static mixer as a function of injection location and flow ratio. *Polym. Engng Sci.* **43**, 875–890.